Contents lists available at ScienceDirect

Journal of Wind Engineering & Industrial Aerodynamics

journal homepage: www.elsevier.com/locate/jweia

Highlights

Quantifying complexity in the envelope reconstruction problem: Review, comparison and a detailed illustration

V. Denoël

Journal of Wind Engineering & Industrial Aerodynamics xxx (xxxx) xxx

- Comprehensive review of methods for determining Equivalent Static Wind Loads.
- Introduction of Aerodynamic-Structural Complexity for envelope reconstruction.
- Optimal ESWLs derived via principal component analysis.
- Future directions: non-symmetric envelopes, nonlinear responses, AI optimization.

AUTHOR PREPRINT VERSION

Quantifying Complexity in the Envelope Reconstruction Problem: review, comparison and a detailed illustration

V. Denoël

Structural & Stochastic Dynamics, University of Liège

Abstract

This document serves as an extension of the keynote presentation delivered in Florence during the 16th International Conference on Wind Engineering. It elucidates the objectives and reviews the challenges related to two pivotal issues at the juncture of wind and structural engineering: (i) the computation of Equivalent Static Wind Loads and (ii) the reconstruction of the envelope of structural responses. Various existing techniques are examined in this paper, accompanied by practical insights drawn from a simple academic example, accessible as supplementary material. Additionally, the notion of Aerodynamic-Structural Complexity is introduced as a pertinent indicator, effectively capturing the intertwined intricacies of both wind aerodynamics and structural behavior.

Keywords: ESWL, Equivalent Static Wind Load, Principal Static Wind Load, Universal Wind Load, Covariance Proper Transformation

Glossary

Response: Any quantity characterizing the structure's response to dynamic wind loading (displacement, internal forces, reactions, stresses, acceleration, any other design criterion). A response can characterize both a quantity corresponding to a dynamic action or the equivalent static action.

Envelope: Maximum and minimum values assumed by the responses under the effect of wind loading. We refer to the envelope of response under dynamic loading and the envelope of response under the effect of one or more static load cases.

Envelope **Reconstruction**: Process aimed at reconstructing an envelope under a set of static loads to make it as close as possible to the envelope of responses under the dynamic loading.

Complexity: Minimum number of static load cases to consider in order to reconstruct any equivalent static load case through linear combination.

Equivalent **Static Load Case**: Set of statistical load distributions applied to the structure that, when applied, provide the same static response as the maximum dynamic response under dynamic loading.

Nomenclature

$\mathbf{M}$, $\mathbf{C}$, $\mathbf{K}$: mass, damping, and stiffness matrices

$\mathbf{\Phi}_m$, ω_m: structural eigen modes and corresponding circular frequency

wind pressure field $p\left(x,t\right)$

$\mathbf{f}\left(t\right)$: is a space-discretized version (see e.g. [1])

$\mathbf{x}\left(t\right)$: are the nodal displacements of a finite element structural model.

$\mathbf{z}\left(t\right)$: structural responses

$\mathbf{A}$: combination matrix, $\mathbf{a}$ combination vector,

$\mathbf{B}=\mathbf{KA}$: static combination matrix, $\mathbf{b}=\mathbf{Ka}$ static combination vector,

$\mathbf{z}_{\max},\mathbf{z}_{\min}$: actual envelope of responses

$\mathbf{z}_{\text{mean}},\boldsymbol{\sigma}_{\mathbf{z}}$: vector of mean values and standard deviations of responses

g^{+}, g^{-}: peak factors

$\mathbf{\Sigma}_{\mathbf{x}}$: covariance of structural displacements (notice that the mean value is subtracted)

$\mathbf{\Sigma}_{\mathbf{f}}$: covariance of the fluctuating part of wind loads

$\mathbf{\Sigma}_{\mathbf{xf}}$: cross-covariance between aerodynamic loads and displacements reads

$\mathbf{\Sigma}_{\mathbf{zf}}$: cross-covariance between aerodynamic loads and responses

σ_z: standard deviation of a structural response

$\sigma_{f,i}$: standard deviation of the actual aerodynamic loading at a given DOF

$\rho_{zf,i}$: correlation coefficient between a structural response z and the actual aerodynamic loading at a given DOF

$\mathbf{S}_{\mathbf{x}}\left(\omega\right)$: PSD of structural displacements

$\mathbf{S}_{\mathbf{xf}}\left(\omega\right)$: cross-power spectral density matrix between structural displacements and applied loads.

$\mathbf{S}_{\mathbf{zf}}\left(\omega\right)$: cross-power spectral density matrix between structural responses and applied loads.

σ_{z_m}: standard deviation of the modal structural response $z_m(t)$

$\sigma_{q,m}$: standard deviation of the modal response $q_m(t)$

$\rho_{q,mn}$: correlation coefficient between modal responses $q_m(t)$ and $q_n(t)$ in modes m and n

$\mathbf{f}_{\mathrm{E}}^{+}$, $\mathbf{f}_{\mathrm{E}}^{-}$: equivalent static load

$\mathbf{x}_{\mathrm{E}}^{+}$, $\mathbf{x}_{\mathrm{E}}^{-}$: structural displacements under the equivalent static loads $\mathbf{f}_{\mathrm{E}}^{+}$, $\mathbf{f}_{\mathrm{E}}^{-}$

$\tilde{\mathbf{z}}^{+}$, $\tilde{\mathbf{z}}^{-}$: structural responses under the equivalent static loads $\mathbf{f}_{\mathrm{E}}^{+}$, $\mathbf{f}_{\mathrm{E}}^{-}$ ($\tilde{\mathbf{z}}^{+}=\mathbf{A}\mathbf{x}_{\mathrm{E}}^{+}$, $\tilde{\mathbf{z}}^{-}=\mathbf{A}\mathbf{x}_{\mathrm{E}}^{-}$)

$\mathbf{f}_{\mathrm{E}}^{+,\mathrm{LRC}}$: equivalent static load obtained with the Load-Response Correlation (LRC) method

$\mathbf{f}_{\mathrm{E}}^{+,\mathrm{MIL}}$: equivalent static load obtained with the Modal Inertial Loads (MIL) method

$\mathbf{f}_{E}^{+,\mathrm{DRC}}$: equivalent static load obtained with the Displacement-Response Correlation (DRC) method

λ : scaling coefficient

$\mathbf{f}_{\mathrm{E},0}^{+}$, $\mathbf{f}_{\mathrm{E},0}^{-}$: scaled versions of the equivalent static load

n_{z}: number of structural responses

n: number of loaded degrees-of-freedom

n_{ndof}: number of degrees-of-freedom in the structural model

n_{P}: number of principal modes with non negligible singular value

n_{C}: number of PSWLs considered in the reconstruction algorithm (usually, $n_{\mathrm{C}}\simeq n_{\mathrm{P}}$)

r: number of static load distributions used in a reconstruction sequence

$\mathbf{\Psi}=(\boldsymbol{\psi}_1,\cdots,\boldsymbol{\psi}_{\mathrm{ndof}})$: eigenvectors of the covariance matrix $\mathbf{\Sigma}_{\mathbf{f}}$

$\mathbf{\Sigma}_{\mathbf{f}}^{\star}$: eigenvalues of the covariance matrix $\mathbf{\Sigma}_{\mathbf{f}}$

$w_{\mathrm{R},m}$: resonant weighting factor in mode m

w_{B}: background weighting factor

$\mathbf{f}_{\mathrm{E}}^{(i)}$: i-th equivalent static wind load used in a reconstruction sequence
$\left\{\mathbf{f}_{\mathrm{E}}^{(k)}\right\}$: sequence of ESWLs used in the reconstruction problem
$\mathbf{F}_{\mathrm{E}}$: matrix with a large collection of ESWLs
$\mathbf{F}_{\mathrm{P}}$: matrix with principal static wind loads (PSWLs), sorted from most to less important
$\mathbf{S}$: diagonal matrix with singular values
$\mathbf{V}$: combination coefficients to obtain the ESWLs $\mathbf{F}_{\mathrm{E}}$ from the PSWLs $\mathbf{F}_{\mathrm{P}}$
$\hat{\mathbf{z}}_{\max}$, $\hat{\mathbf{z}}_{\min}$: reconstructed envelopes
$\psi_r\left(\hat{\mathbf{z}}_{\max}-\mathbf{z}_{\max}, \hat{\mathbf{z}}_{\min}-\mathbf{z}_{\min}\right)$: cost function to minimize throughout the reconstruction process

1 Introduction

Buffeting wind loads acting on civil engineering structures manifest as a random, time- and space-varying pressure field impacting wind-exposed areas. An effective approach to managing the dynamics of this pressure field within structural analysis should ideally encompass the dynamic nature of both the solicitation and the resulting structural response.

The exploration of defining Equivalent Static Wind Loads (ESWL) to represent these dynamic solicitations has garnered interest in the past and continues to do so for practical reasons. The potential simplification of a complex dynamic analysis into a static one offers structural engineers the convenience of employing their familiar design tools and software. Moreover, when wind is treated as a static loading, it seamlessly integrates with other load cases, such as live loads or snow. The document summarizes various methods for determining ESWL, presenting engineers with diverse approaches to address this complexity. In Section 3, this document reviews and classifies existing methods.

Traditionally, communication between structural and wind engineers halted at the level of ESWLs. However, the ultimate goal of structural design is to ascertain design values for structural responses, including internal forces, displacements, accelerations, and ground reactions. This leads to the crux of the matter—determining a set of ESWLs that closely approximates the envelope of responses under actual dynamic pressure fields, a task termed "the envelope reconstruction problem" [2, 3]. Section 5 provides an in-depth exploration of this challenge.

Throughout our pursuit of this goal, we discovered that Aerodynamic-Structural Complexity, as defined in Section 4, proves to be a simple and robust concept for solving the envelope reconstruction problem. Further details reveal that this indicator originates from the proper orthogonal decomposition of a matrix incorporating a large number of ESWLs. It encompasses the intricacies of both structural behavior and aerodynamic loading, each with its distinct complexity. This paper develops this novel concept through a review of existing techniques for establishing and leveraging ESWLs within the envelope reconstruction framework. Additionally, Section 6 provides an integrated academic illustration, facilitating a comparison of existing techniques using a benchmark example.

Lastly, Section 8 synthesizes major observations and outlines key directions for buffeting analysis and the design of civil engineering structures.

2 Structural Analysis

Let a given pressure field $p\left(x,t\right)$ be measured in a wind tunnel, or possibly computed with CFD simulations. This pressure field acts on a structure whose linear dynamic behavior is characterized by the mass, damping, and stiffness matrices $\mathbf{M}$, $\mathbf{C}$, $\mathbf{K}$. The structural analysis consists in solving

$$\mathbf{M}\ddot{\mathbf{x}}(t) + \mathbf{C}\dot{\mathbf{x}}(t) + \mathbf{K}\mathbf{x}(t) = \mathbf{f}(t) \tag{2.1}$$

where $\mathbf{f}(t)$ is a space-discretized version (see e.g. [1]) of the buffeting loads corresponding to the pressure field $p(x,t)$, and $\mathbf{x}(t)$ are the nodal displacements of a finite element structural model. The dot operator denotes differentiation with respect to time t. Then, structural responses are computed as linear combinations of structural displacements

$$\mathbf{z}(t) = \mathbf{A}\mathbf{x}(t). \tag{2.2}$$

Matrix $\mathbf{A}$ is chosen in such a way that these recombined quantities correspond to the important information for the structural design, e.g. internal forces, displacements or ground reactions. If only one response is considered, this equation becomes

$$z(t) = \mathbf{a}^T\mathbf{x}(t). \tag{2.3}$$

These two equations form the simplest case to be studied. A more advanced problem could include aeroelastic phenomena [4] in the governing equation (2.1), which would then read

$$\left[-\mathbf{M}(\omega)\,\omega^2 + \mathrm{i}\omega\mathbf{C}(\omega) + \mathbf{K}(\omega)\right]\mathbf{X}(\omega) = \mathbf{F}(\omega), \tag{2.4}$$

in the Fourier domain. In this model, buffeting loads are gathered in $\mathbf{F}(\omega)$ while self-excited aeroelastic effects contribute to frequency-dependent matrices. This problem can be solved in the frequency domain to determine the statistics of structural displacements $\mathbf{x}(t)$ [5, 6], which constitute the basic information for the following analysis.

As a second refinement of the basic problem (2.1)-(2.2), nonlinear responses other than the simple linear combination (2.2) could also be considered. For example, Von Mises stresses are obtained as a nonlinear transformation of internal forces. This represents a more complicated problem, which is discussed in Section 5.5. Additionally, Eq. (2.2) is a memoryless transformation, while design quantities could also involve derivatives, delays, or convolutions of the responses. For instance, velocities or accelerations could play a crucial role in the design, a situation discussed in Section 5.5.

Before touching advanced topics, the main part of this paper focuses on the envelope reconstruction of responses from the problem composed of Eqs. (2.1)-(2.2). The foundational information for the envelope reconstruction problem involves structural analysis, i.e., solving Eq. (2.1) or determining structural displacements. This can be achieved in various ways based on the time histories collected in the vector of external forces. The different methods can be classified into families, either in the time [7, 8] or frequency domain [5, 7, 9], and either in the nodal [7] or modal [7] basis. Additionally, in the frequency domain, they can be based on generic numerical integration of power spectral densities [10, 5], or on the background and resonant decomposition [11] and some of its extensions [12, 13]. For simple structures, the equivalent spectrum technique provides very accurate estimates of structural responses [14, 15, 16, 17]. The spatio-temporal nature of the wind loading can also be tackled with the pseudo-excitation method [18]. This analysis method was borrowed from seismic engineering [19] and successfully applied in wind engineering [20]. Lastly, although it is common to assume that the response is Gaussian, simplifying the process of determining the envelope of extreme (design) values, more recent works have also considered the possible non-Gaussian nature of responses [21, 22, 23]. This particular aspect will be discussed in Section 5.5 too.

For now it is assumed that the dynamic structural analysis is performed with one of these techniques of integration and that the corresponding envelope is known. A processing of the data in the time domain would yield the time history of structural displacements $\mathbf{x}(t)$, then of structural response $\mathbf{z}(t)$, and the upper and lower envelopes are defined by

$$\mathbf{z}_{\max} = \max_t \mathbf{z}(t) \qquad ; \qquad \mathbf{z}_{\min} = \min_t \mathbf{z}(t)\,. \tag{2.5}$$

Similarly, in a frequency domain approach, extreme value analysis [24, 25] provides statistical estimates of extreme values.

$$\mathbf{z}_{\max} = \mathbf{z}_{\text{mean}} + g^{+}\boldsymbol{\sigma}_{\mathbf{z}} \qquad ; \qquad \mathbf{z}_{\min} = \mathbf{z}_{\text{mean}} - g^{-}\boldsymbol{\sigma}_{\mathbf{z}} \tag{2.6}$$

where $\mathbf{z}_{\text{mean}}$ collects the mean responses (if not already treated separately) and $\boldsymbol{\sigma}_{\mathbf{z}}$ collects the standard deviations of responses.

Various models of different complexities are available for estimating the peak factors, g^{+} and g^{-}. In a Gaussian context where the response is statistically symmetric ($g^{+} = g^{-}$), an approximation of the peak factor based on the zero up-crossing rate is available [26], and still commonly used today. However, in numerous scenarios where the non-Gaussian nature of loading and response is significant —such as in the design of local cladding elements and short bridges with non-streamlined cross-sections— advanced extreme value models become essential [27]. One option is to employ translation models [28, 21] for instance with the improved moment-based Hermite model [29, 30], or resort to mixed distributions [31]. In time domain approaches, alternative approaches are available, such as the peaks-over-threshold method [32] and the average conditional exceedance rate method [33]. No matter the way the upper and lower envelopes of structural response are determined, they represent the target values that static equivalent wind loads should be capable of reproducing. At this juncture, it is assumed that these envelopes are available and computed independently. Most of the following discussion deals with $z_{\max}$ since in a Gaussian (or symmetric) context, the management of $z_{\min}$ follows the same reasoning.

Besides, the structural analysis provides a series of information that could be useful for the reconstruction of the envelope. Among others, the covariance of structural displacements

$$\boldsymbol{\Sigma}_{\mathbf{x}} = \frac{1}{T}\int_0^T \mathbf{x}(t)\,\mathbf{x}^T(t)\,\mathrm{d}t = \int_{-\infty}^{+\infty} \mathbf{S}_{\mathbf{x}}(\omega)\,\mathrm{d}\omega \tag{2.7}$$

is computed from the time series of displacements $\mathbf{x}(t)$ in the time domain, or from the cross-power spectral density matrix $\mathbf{S}_{\mathbf{x}}(\omega)$ (with double-sided convention here). Also the cross-covariance between aerodynamic loads and displacements reads

$$\boldsymbol{\Sigma}_{\mathbf{xf}} = \frac{1}{T}\int_0^T \mathbf{x}(t)\,\mathbf{f}^T(t)\,\mathrm{d}t = \int_{-\infty}^{+\infty} \mathbf{S}_{\mathbf{xf}}(\omega)\,\mathrm{d}\omega \tag{2.8}$$

where $\mathbf{S}_{\mathbf{xf}}(\omega)$ is the cross-power spectral density matrix between structural displacements and applied loads. Similarly,

$$\boldsymbol{\Sigma}_{\mathbf{zf}} = \frac{1}{T}\int_0^T \mathbf{z}(t)\,\mathbf{f}^T(t)\,\mathrm{d}t = \int_{-\infty}^{+\infty} \mathbf{S}_{\mathbf{zf}}(\omega)\,\mathrm{d}\omega \tag{2.9}$$

represents the cross-covariance between aerodynamic loads and responses. References on dedicated stochastic analysis [34] specify that if $\mathbf{S}_{\mathbf{f}}(\omega)$ denotes the cross-power spectral density matrix of wind loads and $\mathbf{H}(\omega) = \left[-\mathbf{M}\omega^2 + \mathrm{i}\omega\mathbf{C} + \mathbf{K}\right]^{-1}$ is the structural frequency response function, the following relationships hold:

$$\mathbf{S}_{\mathbf{x}}(\omega) = \mathbf{H}(\omega)\,\mathbf{S}_{\mathbf{f}}(\omega)\,\bar{\mathbf{H}}^T(\omega) \quad ; \quad \mathbf{S}_{\mathbf{xf}}(\omega) = \mathbf{H}(\omega)\,\mathbf{S}_{\mathbf{f}}(\omega) \quad ; \quad \mathbf{S}_{\mathbf{zf}}(\omega) = \mathbf{A}\,\mathbf{H}(\omega)\,\mathbf{S}_{\mathbf{f}}(\omega)\,. \tag{2.10}$$

3 Equivalent Static Wind Loads

3.1 Definition

An equivalent static load $\mathbf{f}_\mathrm{E}^{\pm}$ is a distribution of static loads that allows for the reproduction of a response identical to what would have been obtained by considering dynamic wind loading. Specifically, for the upper envelope (+) of a given response $z_{\max} = \max_t \mathbf{a}^T \mathbf{x}(t)$,

$$\mathbf{f}_\mathrm{E}^{+} \text{ is such that } \mathbf{K}\mathbf{x}_\mathrm{E}^{+} = \mathbf{f}_\mathrm{E}^{+} \text{ provides } \mathbf{x}_\mathrm{E}^{+} \text{ such that } \mathbf{a}^T\mathbf{x}_\mathrm{E}^{+} = z_{\max}. \tag{3.1}$$

It is subtilely different from an equivalent static wind load (ESWL), which, by incorporating an additional qualifier, refers to a load distribution expected to mimic realistic wind conditions. While general structural analysis consists in calculating responses under given loads, the determination of ESWL aims at determining loads for given responses.

Their mathematical definition is unfortunately poorly posed, and there is no unique solution to this problem. This is evident when considering that the equivalent load may have as many degrees of freedom as in the structural model (since any node could be loaded), while the equivalence is based on just a scalar equation. Therefore, there exists an infinity of solutions to this problem, at least as long as no additional constraint is added. To address this, the definition $\mathbf{x}_\mathrm{E}^{+} = \mathbf{a}^\dagger z_{\max}$ is introduced, where $\mathbf{a}^\dagger$ is a pseudo-inverse of $\mathbf{a}$, such that $\mathbf{a}^T\mathbf{a}^\dagger = 1$, and

$$\mathbf{f}_\mathrm{E}^{+} = \mathbf{K}\mathbf{a}^\dagger z_{\max} \qquad ; \qquad \mathbf{f}_\mathrm{E}^{-} = \mathbf{K}\mathbf{a}^\dagger z_{\min}. \tag{3.2}$$

To better condition the problem, one could consider a straightforward solution by increasing the number of responses for which equivalence must be established. By doing so, the number of solicitations to be determined should correspond to the number of responses to reproduce. This approach enables the formation of a system with as many equations as unknowns, resulting in $\mathbf{A}$ being square. Consequently,

$$\mathbf{f}_\mathrm{E}^{+} = \mathbf{K}\mathbf{A}^{-1}\mathbf{z}_{\max} \qquad ; \qquad \mathbf{f}_\mathrm{E}^{-} = \mathbf{K}\mathbf{A}^{-1}\mathbf{z}_{\min}. \tag{3.3}$$

Unfortunately, there is no guarantee that this system of equations is better conditioned, i.e. that $\mathbf{A}^{-1}$ exists. The question of conditioning is discussed in Section 3.2.

When ESWLs were initially derived [35, 36, 37] , the notion of establishing them for every conceivable response in a large structural model was deemed impractical. Creating a system with $\mathbf{A}$ square and perfectly well-conditioned was beyond the scope at that time. The prevailing approach, from early times until recent years, involved determining ESWLs for only a few selected responses, upon which the structural design was then based.

A fundamental aspect in the theory of ESWLs revolves around deriving an ESWL for a single response, a topic explored later in this Section. Given the absence of a unique solution to the definition of ESWLs, efforts were directed early on towards defining them with specific properties. One such property relates to the crucial non-overshooting conditions, rendering ESWLs valuable in the envelope reconstruction problem. This particular property is discussed in Section 3.3.

3.2 On the well-posedness of the determination of ESWL

The well-posedness of the derivation of ESWLs is discussed with a simple 2-DOF example. This famous example [38] is made as simple as possible to understand the point with simple arguments. Let's consider the 2-DOF double cantilever structure shown in Figure 3.1. The two DOFs correspond to the along-wind displacements of cantilever ends, $\mathbf{x} = (x_1, x_2)^T$. The stiffness matrix of this simple structure is

$$\mathbf{K} = \frac{1}{2}\begin{pmatrix} k_\mathrm{B} + k_\mathrm{T} & k_\mathrm{B} - k_\mathrm{T} \\ k_\mathrm{B} - k_\mathrm{T} & k_\mathrm{B} + k_\mathrm{T} \end{pmatrix} \tag{3.4}$$

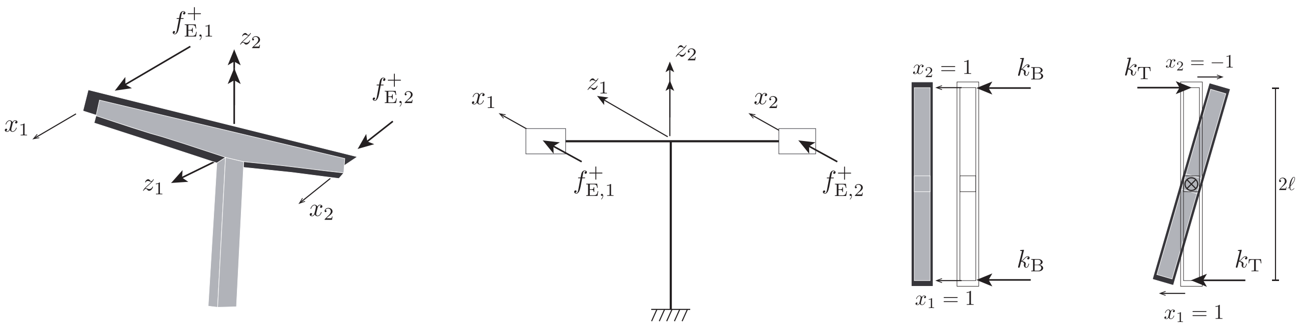

Fig. 3.1: A cantilever bridge under construction idealized as a 2-DOF structure; example used to illustrate the non-uniqueness of the problem.

where k_B and k_T are related to the bending and torsional stiffnesses of the pile, respectively. The along-wind displacement $z_1(t) = \mathbf{a}_1^T \mathbf{x}(t)$ of the top of the pile is a typical response of interest. It is obtained by linear interpolation between x_1 and x_2, i.e. $z_1(t) = \left(\frac{1}{2}, \frac{1}{2}\right) \mathbf{x}(t)$. The generic pseudo-inverse of $\mathbf{a}_1$ is $\mathbf{a}_1^\dagger = (1+\alpha, 1-\alpha)^T$ where $\alpha \in \mathbb{R}$. It is indeed such that $\mathbf{a}_1^T \mathbf{a}_1^\dagger = 1$, $\forall \alpha$. A specific choice is for instance ($\alpha = 0$), $\mathbf{a}_1^\dagger = (1,1)^T$. A given along-wind displacement $z_{\max,1}$ can be recovered with the static equivalent wind load $\mathbf{f}_\mathrm{E}^+ = \mathbf{K}\mathbf{a}_1^\dagger z_{\max,1} = k_\mathrm{B}(1,1)^T z_{\max,1}$, which consists of two equal loads applied at both ends of the cantilever. In the general case $\alpha \in \mathbb{R}$, one has $\mathbf{f}_\mathrm{E}^+ = \mathbf{K}\mathbf{a}_1^\dagger z_{\max,1} = (k_\mathrm{B} + \alpha k_\mathrm{T}, k_\mathrm{B} - \alpha k_\mathrm{T})^T z_{\max,1}$, meaning that the same maximum displacement of the top of the pile can be obtained with any additional torque. This load case is however accompanied by a rotation since the displacements at the ends of the cantilevers are not equal any longer. This illustrates the non-uniqueness of the equivalent static loading.

By considering a second response, $z_2(t) = \left(-\frac{1}{2\ell}, \frac{1}{2\ell}\right) \mathbf{x}(t)$, the torsional response of the deck, it is possible to seek the determination of the equivalent static loading that recovers both the bending ($z_{\max,1} \equiv \delta_{\max}$) and the torsional ($z_{\max,2} \equiv \theta_{\max}$) responses at the same time. With the notations introduced above $\mathbf{A} = \left(\frac{1}{2}, \frac{1}{2}; -\frac{1}{2\ell}, \frac{1}{2\ell}\right)$, and

$$\mathbf{K}\mathbf{A}^{-1} = \begin{pmatrix} k_\mathrm{B} & -\ell k_\mathrm{T} \\ k_\mathrm{B} & \ell k_\mathrm{T} \end{pmatrix} \quad \rightarrow \quad \mathbf{f}_\mathrm{E}^+ = \begin{pmatrix} k_\mathrm{B} z_{\max,1} - \ell k_\mathrm{T} z_{\max,2} \\ k_\mathrm{B} z_{\max,1} + \ell k_\mathrm{T} z_{\max,2} \end{pmatrix}. \tag{3.5}$$

Adding a second response, the determination of the equivalent static loading is now well posed. This is because the combination matrix $\mathbf{A}$ is square and non-singular ($\det \mathbf{A} = 1/(2\ell)$), i.e. invertible. This of course shall not be the case for any square matrix. In other words, it is not sufficient to form a problem with as many responses as degrees-of-freedom.

As a counter-example, it is straightforward to imagine another configuration where the second response would be the along-wind displacement of the pile at mid-height, while there is no torsional response anymore. Using a (perhaps too simple) interpolation between the base and the top, invoking for instance the fact that the structure behaves in a simple quasi-static way, the second response would read $z_2(t) = \mathbf{a}_2^T \mathbf{x}(t) = \left(\frac{1}{4}, \frac{1}{4}\right) \mathbf{x}(t)$. It is clear that $\mathbf{A} = \left(\mathbf{a}_1^T; \mathbf{a}_2^T\right)$ is now singular. As a consequence, there is an infinite set of equivalent static loads able to provide the along-wind displacements at the top ($\delta_{\max}$) and at mid-height ($\delta_{\max}/2$) at the same time. Two responses are considered, but they are not sufficient to solve the non-uniqueness issue. After the concept of complexity will be introduced in Section 4, it will be clear that the determination of one ESWL to recover two responses doesn't have a unique solution when the complexity is equal to 1.

Furthermore, since the maximum responses $z_{\max,1}$ and $z_{\max,2}$ don't happen at the same time, and even more at times different from those when $x_{\max,1}$ and $x_{\max,2}$ are reached, the maximum values $x_{\max,1}$ and $x_{\max,2}$ are not necessarily reached under the equivalent static wind load defined above.

This example is simple enough to understand that the conditioning of the determination of ESWLs depends on the invertibility of $\mathbf{A}$. In more complicated structures and wind loadings, the same reasoning is not necessarily obvious and usage of mathematical tools available in algebra are helpful to determine the conditioning of the problem.

3.3 The equivalence and non-overshooting conditions

Since the determination of the optimal number of responses appears to be a non-trivial task (addressed in Section 4), and computational challenges made it cumbersome in the early stages of ESWLs, it has become customary to consider one response at a time, i.e., based on (2.3) instead of (2.2). It is now evident that many load distributions can reproduce a single response $z_{\max}$, given the non-uniqueness of the pseudo-inverse $\mathbf{a}^{\dagger}$. Various solutions to this issue are presented in the rest of this section, each corresponding to a load distribution $\mathbf{f}_{\mathrm{E}}^{+} = \mathbf{K}\mathbf{a}^{\dagger} z_{\max}$.

Although established for a single response, this static load distribution can be employed to evaluate responses beyond the one initially considered for determining $\mathbf{f}_{\mathrm{E}}^{+}$. All (other) responses corresponding to application of the static loads $\mathbf{f}_{\mathrm{E}}^{+}$ are

$$\tilde{\mathbf{z}}^{+} = \mathbf{A}\mathbf{x}_{\mathrm{E}}^{+} = \mathbf{A}\mathbf{K}^{-1}\mathbf{f}_{\mathrm{E}}^{+} = \mathbf{A}\mathbf{a}^{\dagger} z_{\max}. \tag{3.6}$$

The combination matrix $\mathbf{A}$ is a collection of combination coefficients $\mathbf{A}_{ji}$, $j = 1, \cdots, n_{\mathrm{z}}$, $i = 1, \cdots, n_{\mathrm{ndof}}$ corresponding to the n_{z} responses resulting from loads applied at the n_{dof} degrees-of-freedom of the structural model (or possibly just part of it).

3.3.1 Equivalence (tangency) condition

The equivalence condition (also called tangency condition) requires that $\tilde{\mathbf{z}}_{j_1} = z_{\max}$ if j_1 represents the response that has been used to determine the equivalent static wind loads $\mathbf{f}_{\mathrm{E}}^{+}$. Since the j_1-th line of $\mathbf{A}$ is $\mathbf{a}^{T}$, the equivalence condition is satisfied as soon as the ESWL is defined as $\mathbf{f}_{\mathrm{E}}^{+} = \mathbf{K}\mathbf{a}^{\dagger} z_{\max}$ where $\mathbf{a}^{\dagger}$ is a pseudo-inverse of $\mathbf{a}$ ($\mathbf{a}^{T}\mathbf{a}^{\dagger} = 1$). In such cases, the equivalence condition is met.

In some other situations, the ESWL $\mathbf{f}_{\mathrm{E}}^{+}$ is defined as a scaled version of a chosen load distribution $\mathbf{f}_{\mathrm{E},0}^{+}$,

$$\mathbf{f}_{\mathrm{E}}^{+} = \lambda \mathbf{f}_{\mathrm{E},0}^{+}, \tag{3.7}$$

and the scaling coefficient λ is chosen in such a way that the equivalence condition is satisfied. For instance, for the upper envelope,

$$\tilde{z}^{+} = \mathbf{a}^{T}\mathbf{K}^{-1}\mathbf{f}_{\mathrm{E}}^{+} = z_{\max} \quad \rightarrow \quad \lambda = \frac{z_{\max}}{\mathbf{a}^{T}\mathbf{K}^{-1}\mathbf{f}_{\mathrm{E},0}^{+}}. \tag{3.8}$$

This option is developed in Sections 3.4.1, 3.4.2 and 3.6.

3.3.2 Non-overshooting condition

More importantly, the non-overshooting condition states that the actual envelope $(\mathbf{z}_{\min,j}; \mathbf{z}_{\max,j})$ for $j = 1, \cdots, n_{\mathrm{z}}$, is nowhere exceeded when the ESWL is applied, or in other words that the responses $\tilde{\mathbf{z}}^{-}$ and $\tilde{\mathbf{z}}^{+}$ obtained under $\mathbf{f}_{\mathrm{E}}^{-} = \mathbf{K}\mathbf{a}^{\dagger} z_{\min}$ and $\mathbf{f}_{\mathrm{E}}^{+} = \mathbf{K}\mathbf{a}^{\dagger} z_{\max}$ are such that

$$\mathbf{z}_{\min,j} \leq \tilde{\mathbf{z}}_{j}^{-} \leq \tilde{\mathbf{z}}_{j}^{+} \leq \mathbf{z}_{\max,j} \qquad \text{for } j = 1, \cdots, n_{\mathrm{z}}. \tag{3.9}$$

The ESWLs $\mathbf{f}_{\mathrm{E}}^{-}$ and $\mathbf{f}_{\mathrm{E}}^{+}$ play a crucial role in replicating extreme values for response j_1. Violating the non-overshooting condition would lead the design engineer to overestimate responses at other locations in the structure when applying these load cases. While a slight overestimation may not be a major concern, exceeding 10% or even 20% could pose significant issues. In such scenarios, certain elements in the structure, especially secondary elements, would be subjected to larger loads than intended, resulting in an uneconomical design. When overshooting is not avoidable, at least it would be interesting to make it as small as possible. This, of course, depends on the considered problem and the method used to determine ESWLs.

Conversely, if the responses generated by $\mathbf{f}_{\mathrm{E}}^{-}$ and $\mathbf{f}_{\mathrm{E}}^{+}$ are significantly lower than their actual response values $\mathbf{z}_{\mathrm{min},j}$ and $\mathbf{z}_{\mathrm{max},j}$, it indicates that these static wind loads inadequately reconstruct the actual envelope. In an ideal situation, the considered load cases $\mathbf{f}_{\mathrm{E}}^{-}$ and $\mathbf{f}_{\mathrm{E}}^{+}$ would reconstruct the envelope accurately across the entire structure with limited under- and over-estimations of the envelope. As explored later, achieving this perfect reconstruction is only possible when the Structural−Aerodynamic Complexity is equal to 1. Meanwhile, it is noteworthy that this objective was central to the establishment of the Universal Wind Load [39, 40], aiming to replicate the entire envelope with only one load distribution, as effectively as possible.

The discussion of envelope reconstruction is deferred to Section 5. In the remainder of this Section, various methods for establishing ESWLs are presented together with their non-overshooting or bounding capabilities.

3.4 ESWLs based on the wind pressure only

For wind engineers immersed in wind tunnel studies, a distinctive advantage lies in the ability to exclusively handle wind data without the necessity of owning the structural model. Indeed, analyzing the wind flow provides a foundational understanding of the prevailing wind patterns, unencumbered by the complexities associated with structural intricacies. In this scenario, the initial and often preferred method involves processing either the mean wind flow [11, 36] or solely the covariance of the wind pressure fluctuations [41, 42].

This method not only simplifies the analytical process but also splits responsibilities between the wind and structural engineer aligning with the practical reality, at least until late 1990s. In this initial method, several variants come into play, each offering distinct perspectives on wind behavior. The mean wind pressure field serves as a fundamental starting point, providing insights into the prevailing pressure patterns induced by the wind. Building upon this, the covariance proper transformation (CPT) of the pressure fluctuation takes a more detailed approach, delving into the statistical relationships and fluctuations within the pressure field. These two approaches are detailed in the rest of this section.

Expanding the toolkit, the Spectral Proper Transformation adds a spectral dimension to the analysis, offering a frequency-based exploration of the pressure fluctuations. Beyond these core methods, various extensions emerged leveraging techniques such as Proper Orthogonal Decomposition (POD), in its original version [43, 44] or in one of its numerous variants [45, 46], or based on Dynamic Mode Decomposition (DMD) [47], and other modal analysis approaches [48].

3.4.1 The mean wind flow and the gust response factor

As a first approach, the unscaled ESWLs can be defined as

$$\mathbf{f}_{\mathrm{E},0} = \mathbf{f}_{\mathrm{mean}} = \frac{1}{T}\int_{0}^{T} \mathbf{f}\,(t)\,\mathrm{d}t \tag{3.10}$$

where $\mathbf{f}_{\text{mean}}$ represents the average wind load field on the considered structure. Applying these loads to the structure yields the average responses $\mathbf{z}_{\text{mean}}$, which differ from $\mathbf{z}_{\max}$ and $\mathbf{z}_{\min}$ as seen in Eq. (2.6). Therefore, it is essential to scale $\mathbf{f}_{\text{E},0}$ with the appropriate load multiplier λ, as explained in Section 3.3.1. If the standard deviation $\boldsymbol{\sigma}_{\mathbf{z}}$ is proportional to the mean response $\mathbf{z}_{\text{mean}}$ and if the peak factors g^+ and g^- are unique for all considered structural responses, this load multiplier corresponds to the gust response factor, i.e. the quantity by which the mean wind loads need to be multiplied to reconstruct the envelope everywhere.

The conditions for the gust response factor approach to be applicable are quite strict. While the latter is often overlooked, and the the statistical symmetry of the loading is hidden behind an assumption of Gaussianity, the former is more severe. Besides a single-DOF structure loaded at one point, the condition $\boldsymbol{\sigma}_{\mathbf{z}} \propto \mathbf{z}_{\text{mean}}$ is a mere assumption. It is not problematic, though, when the size of the structure remains small and, in case of resonant response, when the sign of mode shapes remains identical along the entire structure. Because of its simplicity, the gust response factor is used in codification procedures [49, 50]. It has been used and applied on a regular basis. The advantages and limitations have been summarized by Kareem and Zhou [51]. It is convenient for the along wind structural response [52]. Examples of application concern transmission lines [53], long span roofs [54, 55, 56, 57, 58], large cooling towers [59]. Since this method consists in amplifying the mean wind field by an ad hoc scaling factor, it is inappropriate to recover a zero-average response; this is the reason why it is recommended not to use it in case of zero-crossing influence lines or modal responses. Some of the following methods shall be applied in this case.

3.4.2 Covariance proper transformation

A second approach is rooted in the Proper Orthogonal Decomposition (POD) of the covariance matrix of wind loads. In this specific case, the POD involves the eigenvalue decomposition

$$\boldsymbol{\Sigma}_{\mathbf{f}} = \frac{1}{T}\int_0^T \left(\mathbf{f}\left(t\right) - \mathbf{f}_{\text{mean}}\right)\left(\mathbf{f}\left(t\right) - \mathbf{f}_{\text{mean}}\right)^T \mathrm{d}t = \boldsymbol{\Psi}\boldsymbol{\Sigma}_{\mathbf{f}}^{\star}\boldsymbol{\Psi}^T \tag{3.11}$$

where $\boldsymbol{\Psi} = (\boldsymbol{\psi}_1, \cdots, \boldsymbol{\psi}_{\text{ndof}})$ and $\boldsymbol{\Sigma}_{\mathbf{f}}^{\star}$ respectively collect the eigenvectors and eigenvalues of the symmetric positive definite covariance matrix $\boldsymbol{\Sigma}_{\mathbf{f}}$ of the fluctuating wind loads. Removing the average wind field before computing the covariance matrix is more efficient [46]. All eigenvalues are positive. When sorted from largest to smallest, the first few corresponding eigenvectors form a sequence of load distributions that can be combined to reconstruct the actual load distribution, at least in terms of its magnitude (variance) and spatial correlation (covariance). In the absence of information about the structural behaviour, these eigenvectors emerge as the optimal candidates for synthesizing the wind loads on the structure.

According to this concept, the unscaled Equivalent Static Wind Loads (ESWL) are defined as

$$\mathbf{f}_{\text{E},0} = \boldsymbol{\Psi}_i, \tag{3.12}$$

with i chosen as $i = 1$ when only one wind loading mode is deemed sufficient to reconstruct the original covariance matrix $\boldsymbol{\Sigma}_{\mathbf{f}}$. Alternatively, one could explore a few subsequent values of i and consider the corresponding loading modes to define alternative ESWLs. Since the POD is employed for data reduction, it is generally less appealing to consider loading modes larger than, say, $i \sim 10$ or maybe a few dozens, except in very specific conditions, as illustrated later.

This method has been used to characterize the wind loading modes on long span bridges [60, 61], long span roofs [62, 63] and tall buildings [64, 65, 66, 46]. The use of the covariance proper transformation is anterior to the envelope reconstruction problem, at least in the format that is presented in Section 5. It is more usual to see the CPT modes being used to explain the wind flow, rather than to use them as ESWLs, except perhaps when there are just a bunch of ESWLs, and the structural behavior remain rather simple.

3.5 The Load-Response Correlation (LRC) and Conditional Sampling Technique (CST)

As a third method, the Load-Response-Correlation defines the Equivalent Static Wind Loads (ESWLs) based on the correlation between wind loads and structural responses. It holds particular appeal due to its intrinsic consideration of the dynamic interaction between wind and structure, unlike other methods that treat wind loads in isolation. The method originated within the research team at Ruhr-Universität Bochum [67, 68], in the continuation of the work initiated earlier by Niemann in the early 1980s [69, 70]. It assumes that the structure responds quasi-statically, implying $\mathbf{x}(t) = \mathbf{K}^{-1}\mathbf{f}(t)$, and Eq. (2.3) becomes $z(t) = \mathbf{b}^T\mathbf{f}(t)$, where $\mathbf{b}^T = \mathbf{a}^T\mathbf{K}^{-1}$. Consequently, the responses are obtained as a memoryless transformation of applied loads, and the dynamic nature of the structural behavior is omitted.

Standard probabilistic theories [34] provide

$$\sigma_z^2 = \frac{1}{T}\int_0^T \mathbf{b}^T\mathbf{f}\,(t)\,z\,(t)\,\mathrm{d}t = \mathbf{b}^T\boldsymbol{\Sigma}_{\mathbf{f}z} = \sum_{i=1}^{n_{\mathrm{dof}}} b_i\rho_{zf,i}\sigma_z\sigma_{f,i} \tag{3.13}$$

where $\sigma_{f,i}$ and $\rho_{zf,i}$ respectively represent the standard deviation of the (zero-mean) wind load at DOF i and the correlation coefficient between that load and the considered response $z\,(t)$. The essence of the method recognizes that the maximum response $z_{\max} = g^+\sigma_z$ is trivially equal to $z_{\max} = g^+\sigma_z^2/\sigma_z$, which yields

$$z_{\max} = g^+\sum_{i=1}^{n_{\mathrm{dof}}} b_i\rho_{zf,i}\sigma_{f,i} = \sum_{i=1}^{n_{\mathrm{dof}}} b_i\left(g^+\rho_{zf,i}\sigma_{f,i}\right). \tag{3.14}$$

Consequently, by defining the ESWL as

$$f_{E,i}^{+,\mathrm{LRC}} = g^+\rho_{zf,i}\sigma_{f,i}, \tag{3.15}$$

it is evident that the response under this ESWL, $\tilde{z}^+ = \mathbf{b}^T\mathbf{f}_E^{+,\mathrm{LRC}}$, is well equal to $z_{\max}$, satisfying the equivalence condition (Section 3.3.1). This short formulation assumes that the average response is treated separately. The complete formulation including the average is presented in [68]. The physical meaning of (3.15) is that the ESWL at DOF i, $f_{E,i}^{+,\mathrm{LRC}}$, corresponds to the most probable load at that DOF, conditioned upon occurrence of the maximum response $z_{\max}$ [71].

In essence, this encapsulates the probabilistic foundation of the Conditional Sampling Technique (CST), a method that extracts ESWLs from wind tunnel data by working directly with time series, rather than relying on a statistically processed version[72, 73, 74]. The CST achieves this by conducting a conditional sampling of wind pressure, contingent upon recovering the maximum responses of interest. Consequently, the CST and LRC methods can be regarded as instantiations of the same probabilistic theory, with the former representing a direct sampled version and the latter its statistically processed instantiation. It could be argued that the CST suffers from sampling issues, but this corresponds to the actual practice of wind tunnel studies. This has not prevented the method to be successively applied in many fields, see e.g. [65, 75, 76, 77].

It has been later demonstrated [78] that the ESWLs derived with the LRC method do not overshoot the envelope provided peak factors are the same for all responses. Indeed, for any other response that would read $z'(t) = \mathbf{b}'^T \mathbf{f}(t)$, the response generated by the ESWL associated with response $z(t)$ is

$$\tilde{z}' = \sum_{i=1}^{n_{\text{dof}}} b_i'^T f_{E,i}^{+,\text{LRC}} = g^+ \sum_{i=1}^{n_{\text{dof}}} b_i'^T \rho_{zf,i} \sigma_{f,i} \leq g^+ \sum_{i=1}^{n_{\text{dof}}} b_i'^T \sigma_{f,i} = z'_{\max}. \tag{3.16}$$

Similarly $z_{\min} \leq \tilde{z}'$, so any response generated by the ESWL $\mathbf{f}_E^{\text{LRC}}$ remains inside the envelope.

Last but not least, from the definition (3.2), it is seen that the ESWL $\mathbf{f}_E^{\text{LRC}}$ corresponds to

$$\mathbf{a}^\dagger = \frac{1}{z_{\max}} \mathbf{K}^{-1} \mathbf{f}_E^{+,\text{LRC}}. \tag{3.17}$$

Some steps are necessary to indeed check that $\mathbf{a}^T \mathbf{a}^\dagger = 1$, starting from $\mathbf{b}^T = \mathbf{a}^T \mathbf{K}^{-1}$. More importantly, it is worth mentioning that the LRC method could be seen as just one specific way to define the pseudo-inverse $\mathbf{a}^\dagger$. However, this specific definition is just one-of-a-kind, as it satisfies de facto the non-overshooting condition (provided the loading and responses are Gaussian, and the response is quasi-static). The LRC method has been mostly applied to structures that are known to have a background response. Low-rise buildings are therefore good candidates [79, 80], although bridges can also be studied [81], or high-rise buildings [82] under some adjustments. Also, the original method has been modified in order to define groups of structural responses that can be reconstructed with an LRC-based approach [83, 84]. This is investigated in more detail in Section 5.

It is now evident that the LRC method presents significant advantages in a linear environment, providing non-overshooting characteristics with minimal constraints such as quasi-static behavior. Moreover, it effectively mirrors the specific trends of a wind loading, stemming from the interpretation of ESWLs as most probable wind load distributions. Nevertheless, while the method has been suggested for use in a nonlinear context [85], the compelling arguments mentioned above unfortunately do not hold any longer.

3.6 The Modal Inertial Loads (MIL)

The LRC and CST methods face two limitations, as demonstrated in a straightforward example: imagine a simply supported beam loaded solely at midspan, for instance with a light highway signboard, see Figure 3.2. Indeed, in the LRC method, equivalent static wind loads are applied only where actual wind loads develop, ie. at midspan only if one neglect the drag on the supporting beam. The resulting Equivalent Static Wind Load (ESWL) would appear as a single point load at midspan, inducing a triangular bending moment. However, if the actual wind loading triggers a resonant response, the deformed configuration resembles the sinusoidal mode shape of a simply supported beam. Consequently, the corresponding bending moment diagram is sinusoidal [7], differing from the triangular bending moment produced by a midspan load.

This example underscores that the precision of the LRC and CST methods is confined to structural responses of the background type. Furthermore, they exclusively provide equivalent loads at degrees-of-freedom physically loaded by the wind, generating only a subset of potential deformed configurations. In particular, these methods might not be suitable for generating deformed configurations proportional to specific mode shapes.

Modal Inertial Loads (MIL) find frequent use in structural engineering analysis and have been employed to define ESWLs by Davenport [36] and Holmes [86]. When applied statically to a structure, MILs generate deformations corresponding to the mode shapes. They are defined as follows:

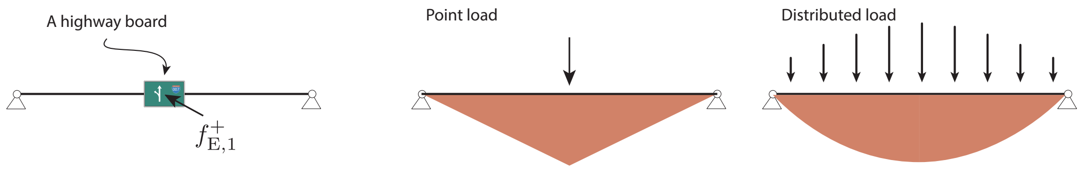

Fig. 3.2: Example of a simply supported beam with a wind loading at midspan only. Some ESWL methods provide loads where the actural wind loads are located (at mid-span), while other methods provide equivalent loads distributed along the entire structure, as a result of inertial forces.

$$\mathbf{p}_m = \mathbf{K}\mathbf{\Phi}_m = \omega_m^2 \mathbf{M}\mathbf{\Phi}_m \tag{3.18}$$

where ω_m corresponds to the $m-$th natural frequency. If we assume the response takes place in only one mode with a known standard deviation σ_{q_m}, the MIL-based ESWL $\mathbf{f}^{\mathrm{MIL}}_{E,m} = g^+ \sigma_{q_m} \mathbf{p}_m$ is obtained. The displacement field $\mathbf{x}_E = g^+ \sigma_{q,m} \mathbf{\Phi}_m$ generated by $\mathbf{f}^{\mathrm{MIL}}_{E,m}$ is proportional to the mode shape $\mathbf{\Phi}_m$, and thus, the reconstructed response is given by

$$\tilde{z} = \mathbf{a}^T \mathbf{x}_E = \sigma_{q,m} \mathbf{a}^T \mathbf{\Phi}_m = \sigma_{q,m} \mathbf{a}^T \mathbf{K}^{-1} \mathbf{p}_m = \mathbf{b}^T \mathbf{f}^{\mathrm{MIL}}_{E,m}. \tag{3.19}$$

This formulation highlights similarities with the LRC. The distinction between maximum and minimum responses is not emphasized since a statistically symmetric response is implicit in a resonant response. When the response takes place in several modes, the response $z\left(t\right)$ is the sum of several modal contributions, i.e. $z\left(t\right) = \sum_m z_m\left(t\right)$, where $z_m\left(t\right) = \mathbf{a}^T \mathbf{\Phi}_m q_m\left(t\right) = \mathbf{b}^T \mathbf{K}\mathbf{\Phi}_m q_m\left(t\right) = \mathbf{b}^T \mathbf{p}_m q_m\left(t\right)$. Since the $z_m\left(t\right)$ are just memoryless transformations of modal coordinates $q_m\left(t\right)$, the correlation coefficients $\rho_{q,mn} = \rho_{z,mn}$ are the same for the modal coordinates and the contributions to the considered response. Consequently from

$$\sigma_z^2 = \sum_{m=1}^{n_{\mathrm{modes}}} \sum_{n=1}^{n_{\mathrm{modes}}} \sigma_{z_m} \sigma_{z_n} \rho_{q,mn} \tag{3.20}$$

and noticing that $\sigma_{z_m} = \mathbf{b}^T \mathbf{p}_m \sigma_{q_m}$, we have

$$z_{\max} = g^+ \frac{\sigma_z^2}{\sigma_z} = g^+ \sum_m \sigma_{z_m} \sum_n \frac{\sigma_{z_n}}{\sigma_z} \rho_{q,mn} = \mathbf{b}^T \left(g^+ \sum_m \sigma_{q_m} \mathbf{p}_m w_{\mathrm{R},m} \right) \tag{3.21}$$

where $w_{\mathrm{R},m} = \sum_n \frac{\sigma_{z_n}}{\sigma_z} \rho_{q,mn}$, so that finally

$$\mathbf{f}^{\mathrm{MIL}}_E = \sum_m w_{\mathrm{R},m} \mathbf{f}^{\mathrm{MIL}}_{E,m} \tag{3.22}$$

The multi-mode ESWL is naturally expressed as a weighted combination of single-mode ESWLs. Regardless of whether a Square Root of the Sum of the Squares (SRSS) combination or a Complete Quadratic Combination (CQC) of modal responses is considered [87, 88], the number of independent load cases is equal to the number of modes, with only the weighting coefficients w_m changing [89].

Comparison with (3.2) indicates that the pseudo-inverse $\mathbf{a}^\dagger$ is now defined as

$$\mathbf{a}^\dagger = \frac{1}{z_{\max}} \mathbf{K}^{-1} \mathbf{f}^{+,\mathrm{MIL}}_E = \frac{1}{z_{\max}} \mathbf{K}^{-1} \lambda \mathbf{f}^{\mathrm{MIL}}_{E,0} = \frac{\lambda}{z_{\max}} \mathbf{\Phi}_m, \tag{3.23}$$

This pseudo-inverse is proportional to the mode shape. Similar to the LRC or CST methods, whose optimal performance is conditioned upon a background response, it's crucial to understand that defining an ESWL with MILs is convenient for reproducing the resonant responses only. For this reasons, it is better suited to relatively light and slender structures, see e.g. [90].

3.7 Combined LRC-MIL loads

The insights gained from the preceding sections underscore that the LRC and MIL approaches are applicable primarily in the two extreme scenarios: where the structural response is either predominantly background or resonant. Recognizing this, a pivotal advancement in the formulation of Equivalent Static Wind Loads (ESWL) involved amalgamating these two concepts. This integration was engineered to yield ESWL formulations applicable across the whole spectrum of cases.

In the late 1980s and thereafter, contributions from researchers such as Davenport and Holmes [36, 37, 91] began representing ESWL in terms of background and resonant load distributions. Although the problem is acknowledged as not well-posed, as discussed in Section 3.2, the prevailing choices were the Load-Response-Correlation (LRC) approach for the background counterpart and Modal Inertial Loads (MILs) for the resonant counterpart. This retrospective preference may be attributed to their tendency to exhibit the non-overshooting property in critical configurations.

Upon decomposing the structural response into background and resonant components, the variance of a response [12, 92], denoted as σ_z^2, is found to consist of two terms. General developments beyond the specific cases outlined for the LRC or MIL-based ESWL reveal the feasibility of expressing ESWL as weighted combinations of these two types of loading. For applications in bridge aerodynamics, Irwin introduced the concept of combining these loadings [93]. This idea was further refined by King [94], who devised an iterative procedure to determine the weighting coefficients. At the same conference, Holmes made another significant stride by addressing the combination of multiple MILs to represent multi-mode resonant responses [86]. Shortly thereafter, Chen and Kareem presented an elegant approach that combines LRC and MILs with appropriate weighting coefficients, accounting for modal correlation [95].

Continuing the derivation from the preceding two sections, the ESWL is expressed as

$$\mathbf{f}_E = w_{\mathrm{B}} \mathbf{f}_E^{\mathrm{LRC}} + \sum_m w_{\mathrm{R},m} \mathbf{f}_{E,m}^{\mathrm{MIL}} \tag{3.24}$$

where $w_{\mathrm{R},m}$ is defined as earlier in Eq. (3.22), and $w_{\mathrm{B}} = \frac{\sigma_{z_b}}{\sigma_z}$. In the current notation, the superscript is omitted as it corresponds to the more general formulation used subsequently. It can be rigorously demonstrated that this formulation of ESWL satisfies both the equivalence and non-overshooting conditions, no matter whether the response is background, resonant or a mix of both. Moreover, it is evident that this weighted combination of Load-Response-Correlation (LRC) and Modal Inertial Loads (MIL) methods converges to LRC and MIL when the structural response tends toward being either background or resonant. In the format presented by Chen and Kareem [95], the background response is obtained in a nodal basis, while the resonant response is determined in a modal basis. Other combinations are also possible, for instance omitting the modal correlations [96], using a modal basis for both the background and resonant contributions, a case which is shown to be less appropriate as to the weak convergence of the modal basis for non-inertial loads [78].

This combined method is applicable to all structures having a intermediate behavior, between quasi-static and resonant, for instance high-rise buildings either in along-wind [97, 98, 99, 100] or in cross-wind response [101] and with the purpose of assessing wind load specifications in code provisions [102, 103, 104, 105], large span roofs [106, 107], bridges [108] for which the background-to-resonant ratio [13] can significantly from mode to mode .

3.8 Other methods based on Load-Response Correlation (LRC) or Displacement-Response Correlation (DRC)

While the ESWL formulation presented in Eq. (3.24) effectively addresses various scenarios, alternative formulations have been proposed. An earlier solution, neglecting modal correlations, was suggested by Holmes [86], representing a specific case of Eq. (3.24) with $w_{\mathrm{R},m} = \frac{\sigma_{z_m}}{\sigma_z}$. More sophisticated formulations within the same background/resonant framework have also been developed, incorporating situations with asymptotically small non-proportional damping [109].

Conceptually, an Equivalent Static Wind Load (ESWL) is a distribution of static loads that, when applied, produces a desired response through static analysis. Responses are expressed as a function of structural displacements, which is the central result of a static analysis. So in principle, the ESWL should be constructed on the basis of the correlation between structural displacements and the response of interest. Under the quasi-static hypothesis though (such as for the LRC approach), structural displacements are uniquely related to internal forces $\mathbf{Kx}$, which are in equilibrium with external loads $\mathbf{p}$. This in fact explains why the LRC method is effective. The situation is similar for MILs, because of their definition 3.18, which indicates that a load is uniquely related to a mode shape.

The more general method coined the Displacement-Response Correlation (DRC) method introduced by Blaise and Denoël [2, 110] suits all situations where the quasi-steady assumption or modal load equivalence are not applicable. In that method, the ESWL is just defined from the most probable displacement field x_{E}, conditioned upon recovery of the maximum response of interest. The DRC based ESWL is then defined from a displacement field as

$$\mathbf{f}_E^{\mathrm{DRC}} = \mathbf{K}\mathbf{x}_{\mathrm{E}}.$$

This definition degenerates into Eq. (3.24) in a Gaussian formulation, and when the background/resonant decomposition is used. It is perhaps slightly more complicated since it requires an exhaustive conditional probability distribution of responses and displacements. It is applicable in a broader context though, in particular when the response is not statistically symmetric any longer. It is able to cope with non-symmetric envelopes, with $g^+ \neq g^-$. Also, by allowing for slight adjustment [111] and controlled over- and under-estimations of the envelope as discussed later, it is also applicable when the peak factor is not unique for the various considered responses [78].

3.9 Universal Wind Loading

The Universal Wind Loading is another central method to determine equivalent static wind loads. In its initial version [39, 40], it is based on time series, and a POD decomposition of a matrix incorporating information about the CPT modes and the influence lines of multiples responses of interest. It has been shown to reproduce simultaneously several responses such as bending moments and shear forces. By gathering information about both the aerodynamic loading and the structural behavior, it possesses the modeling advantages of the double modal transformation [112]. The mathematical developments summarized in section 3.2 indicate that the reconstruction problem can only be solved in a least-square sense when the number of responses is larger than the loading points. In this case, the least-square approach is formulated with the influence lines characterizing the considered responses.

Similar to all other methods, the universal wind loading does not allow for the reconstruction of all possible responses at the same time, especially for large and complex structures such as large shell structures [113]. For structures with large complexity, it is possible, though not systematic, that the distribution of universal equivalent static wind loads may appear unusual, meaning it may not resemble a realistic wind load distribution. In short, although it works well for structures with simple to moderate complexity, additional considerations are necessary for very complex structure, ie. with complex structural behavior or complex aerodynamic loading. Nevertheless, for such structures, it serves as a very good starting point for the envelope reconstruction problem.

It has found several applications, in the field of large reticulated domes [114], large span roofs [115, 116] and emblematic structures [117]. Alternative formulations have been developed to deal with multiple wind components [118].

3.10 Others

The non-Gaussian nature of wind loads on structures is now well recognized [21]. Over the past years, several tools for the structural buffeting analysis have been developed, see e.g. [119] and ESWLs appear as an interesting way to avoid such advanced analysis while offering engineers tools to safely design structures. In such a context, the upper and lower envelopes are different [29] and it is important to distinguish ESWLs with respect to the envelope they aim to reproduce [120]. Joint probability density functions is very high dimensional spaces are an option [121, 122]. Another approach to deal with non Gaussian wind loads and non Gaussian responses is to use the more general DRC method presented earlier [3].

Finally another method, called the Proper Skin Mode, provides yet another means to extract ESWLs. It is rooted on a smoothing of the envelope operator which creates sharp responses [123, 124]. As a result of the smoothing operation, these modes also maintain the appearance of realistic wind load distributions, while being suitable for the envelope reconstruction problem.

3.11 Domains of application

Two recent extensive reviews have been published about ESWL on tall buildings [125] and long span roofs [58]. Interested authors are kindly oriented to these works for an extensive review on the question.

Even if the structural behavior of tall buildings might look simpler than other complex structural systems, there are challenges to be taken as to the determination of equivalent wind loads. In particular, the across-wind vibrations [126, 127], the 3-D nature of the behavior [128, 89] and the combination of along-wind, across-wind and torsional responses [129], the possible structural connections between multiple towers [130], and structural eccentricities [131] are specific features which need to be taken into account. Interestingly the determination of representative wind loads for low-rise buildings has also been formulated in the framework of ESWLs [132, 133, 134]. It should be underlined that works reported in [134] are based on on-site full scale measurements.

The use of ESWL for the design of long span roofs has received probably more attraction than tall buildings due to the broader variety of structural typologies [135, 136]. Indeed, grandstand and stadium roofs [137, 138, 139] behave differently from long span roofs with possible applications to industrial buildings [140, 141], large cantilever roofs [142, 143, 144], and even large domes [145, 146, 147]. The universal wind loading has also found many application in roof system, as discussed earlier, and variants in the time domain [148]. The so-called compensated method has been applied to roof systems [149, 150], and in the scope of the universal wind loading method [151]. Furthermore, the proper skin mode method is also well suited to large roofs [152]. Methods While the LRC method is applicable when the resonant component of the response can be neglected [153], other works highlight the importance of the resonant contribution to the structural response of large span roofs [154]. The question of efficient algorithms for the determination of ESWLs on large roofs is another important question [155]. Last but not least, it is to be underlined that ESWLs have been used to determine the influence of wind loads on specific roof types, in particular, for the design of clip loads on standing seam metal roofs [156, 157].

Beside these two traditional domains of application, tall buildings and large roofs, the concept of ESWLs has also been used for the design of waiting hall buildings of railway stations [158], transmission lines [159, 160], possibly in snow-accreted conditions [161], and other cable structures [162, 163], lattice towers [164, 165], silos [166] and cooling towers [167, 168, 169, 170, 171], or other shell structures [172, 173, 174], arch structures [175], as well as reticulated and deployable structures [176, 177, 178]. Exploratory studies for the design of extra-tall buildings and coupling with gravity effect are other applications treated with ESWLs [179]. There is also an opening demand for wind turbines [180, 181], even if the structural behavior looks simpler, and space structures [182]. Other interesting studies have focused on the influence of a tuned mass damper on the distribution of ESWLs [183], or the influence of a base isolation on a tall building [184].

Anticipating the envelope reconstruction problem, several authors have designed methods to determine ESWLs which are able to reproduce several responses at a time [185, 186, 187, 188]. This aspect will be extensively discussed in Section 5.

4 Aerodynamic-Structural Complexity and Principal Static Wind Loads

4.1 The multi-dimensional nature of ESWLs

As introduced at the beginning of this paper, determining several responses to formulate a closed, well-posed problem is not a simple task for some types of structures, although it is not universally challenging. This is probably why wind engineers and structural engineers have mostly focused on determining just one Equivalent Static Wind Load (ESWL) to reproduce a single response.

In this section, we will discuss which response should be chosen to define the best ESWL. Already in the late 1970s [10], several authors have highlighted that several loadings might be necessary to accurately reproduce the structural responses. For instance, for tall buildings, some argue that reconstructing with ESWL the top displacement only is not necessarily a safe choice (e.g. [189, 102]).

Instead of sorting out which ESWL is the best, we suggest computing them all, a task that is not very difficult with the computational means available today. This means computing ESWLs for all displacements in the structural model (one for each degree-of-freedom), for all internal forces (bending moments, shear forces, axial forces), and for all support forces and moments. All these ESWLs can be stored in a matrix, as

$$\mathbf{F}_{\mathrm{E}} = \left(\mathbf{f}_{\mathrm{E}}^{(1)}, \mathbf{f}_{\mathrm{E}}^{(2)}, \cdots \mathbf{f}_{\mathrm{E}}^{(n_{\mathrm{z}})}\right) \tag{4.1}$$

where n_{z} represents the number of responses. In practice, the matrix has more columns (n_{z} responses) than rows (n_{ndof} loaded DOFs), since all responses are considered.

Figure 4.1 illustrates this idea but is limited to 9 responses: 4 ground reactions (#1-#4), 3 storey displacements (#5-#7), and the bending moments in two cross-sections(#8-#9), just for the sake of simplifying the representation. ESWLs can be determined for each of these responses. One of the many methods summarized in Section 3 can be discussed for this purpose. It is assumed that the project engineer is aware of the limitations and advantages of each approach. Each of these ESWLs can be seen as a vector of loading components at each loaded node, representing a vector in a high-dimensional space. To simplify the representation once more, Figure 4.1 shows the first 3 components $\left(\mathbf{f}_{\mathrm{E},1}^{(i)}, \mathbf{f}_{\mathrm{E},2}^{(i)}, \mathbf{f}_{\mathrm{E},3}^{(i)}\right)$, $i = 1, \cdots, 9$, of the 9 selected ESWLs in a 3-D space. In principle, many more responses are considered, and in a space with many more dimensions.

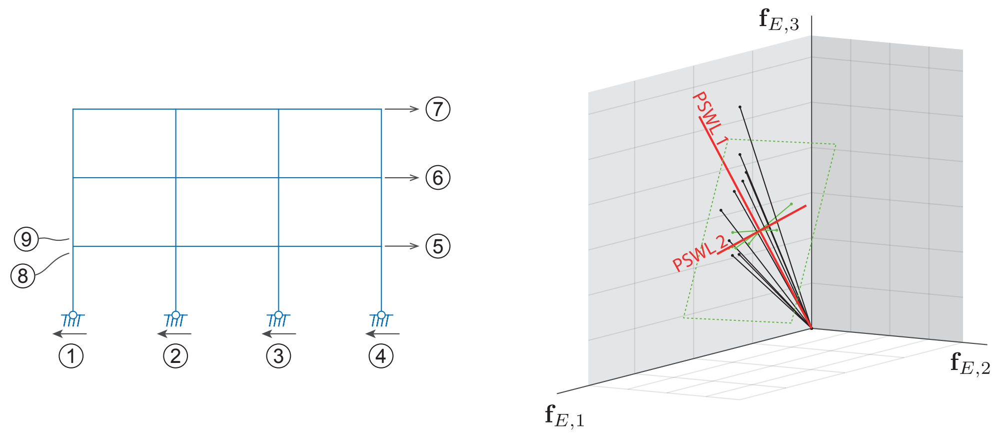

Fig. 4.1: Illustration of the basis of Equivalent Static Wind Loads, and the Principal Static Wind Loads. (Left) Conceptual sketch of a frame structure with 9 responses (ground reactions, storey displacements, bending moments). (Right) Representation of the first 3 components of the ESWLs corresponding to these 9 responses.

It is a key ingredient to recognize that, when keeping all possible responses under the actual wind loading, these vectors exhaustively capture the full Aerodynamic–Structural information of the problem.

4.2 The principal static wind loads (PSWL)

A convenient mathematical basis to represent all ESWLs corresponding to all possible responses in a structure under a given wind loading is the physical basis of structural degrees-of-freedom, $\left(\mathbf{f}_{\mathrm{E}}^{(1)}, \mathbf{f}_{\mathrm{E}}^{(2)}, \cdots \mathbf{f}_{\mathrm{E}}^{(n_{\mathrm{z}})}\right)$, with dimensions $n \times n_{\mathrm{z}}$ where n is the number of degrees-of-freedom where equivalent loads are defined. As illustrated in Figure 4.1, this shall not be the optimal basis for this. Indeed, let's consider a very simple structure, subject to a simple aerodynamic loading, for instance a cantilever beam in the atmospheric boundary layer, a problem that can be studied in closed form [190]. The ESWLs corresponding to the displacements at any level along this beam, as well as those associated with the base shear force and bending moment, look very similar. This translates into vectors representing the ESWLs pointing more or less in the same orientation.

This also reflects the fact that to maximize certain responses, the used equivalent static load cases give distributions that are substantially similar. It is naturally tempting to see if it would be possible to represent all these equivalent static loads in a simpler manner, i.e., by finding the minimum number of independent vectors, forming another mathematical basis, and such that, when recombined adequately, allow reconstructing any of these equivalent loads. From algebra [191, 192], data compression [193, 194], or the prevalent use of POD in wind engineering [41, 42], it is evident that the singular value decomposition of the rectangular ($n \times n_{\mathrm{z}}$) matrix $\mathbf{F}_{\mathrm{E}}$ provides the optimal basis to represent all ESWLs. It reads

$$\mathbf{F}_{\mathrm{E}} = \mathbf{F}_{\mathrm{P}} \mathbf{S} \mathbf{V}^{\mathrm{T}} \tag{4.2}$$

where $\mathbf{S}$ is the $n \times n_{\mathrm{z}}$ matrix of singular values collected along the diagonal, $\mathbf{F}_{\mathrm{P}}$ is the $n \times n$ matrix of corresponding loading modes, and $\mathbf{V}^{\mathrm{T}}$ is the $n_{\mathrm{z}} \times n_{\mathrm{z}}$ matrix of recombination coefficients. In practice, the principal direction can be sought iteratively with one of the several available methods [195]. In the nonlinear iterative partial least squares (NIPALS) approach, the first principal direction is defined as the direction maximizing the projections of all ESWLs. In Figure 4.1, this first direction is illustrated on the right by the red segment labeled "PSWL 1". A first residual is constructed by subtracting from the original set of vectors all components along "PSWL 1". These residuals are illustrated with the green vectors (shifted in the center of the cloud for better visualization). Then, these operations are repeated in the subspace orthogonal to "PSWL-1" (a plane in this case). This yields the definition of "PSWL 2" and repeating this operation in progressively smaller subspaces provides the following principal directions.

With this method, the diagonal elements of $\mathbf{S}$ corresponding to the singular values, $i = 1, \cdots, \min(n, n_z) = n$, are sorted from largest to smallest and, following data compression methods, the information contained in $\mathbf{F}_\mathrm{E}$ can be represented by means of a limited number n_P of principal modes [78, 2]. In typical applications $n_\mathrm{P} \ll \{n, n_z\}$. After truncation, the sizes of the matrices introduced in (4.2) are reduced : $\mathbf{F}_\mathrm{P}$ is $n \times n_\mathrm{P}$, $\mathbf{S}$ is $n_\mathrm{P} \times n_\mathrm{P}$ (now square and diagonal), and $\mathbf{V}^\mathrm{T}$ is $n_\mathrm{P} \times n_z$. Similarly to $\mathbf{F}_\mathrm{E}$ $(n \times n_z)$, matrix $\mathbf{F}_\mathrm{P}$ $(n \times n_z)$ contains a set of equivalent static wind loadings. However, the number of wind load distributions is much smaller, and they can be used to represent, by linear combinations, any of the ESWLs in $\mathbf{F}_\mathrm{E}$, up to a certain accuracy which is controlled by the truncation order.

Being optimal in describing the whole set of ESWLs, the principal static wind loads (PSWLs) have been considered to define the set of static loads that can be used for the structural design and verifications. This concept has been applied by several research groups to large roof structures [188, 196], in combination with ESWL determined with the mixed LRC-MIL method. Other applications to large roof structures are based on the Proper Skin Modes [197].

4.3 The Aerodynamic–Structural Complexity

A convenient method for determining the truncation order used in establishing the basis of PSWLs is to ensure that the cumulative value of the first principal values reaches at least 90% or 95% of the sum of all principal values. This approach closely resembles methods used in other engineering fields. By doing so, the Aerodynamic–Structural Complexity is defined as the number, denoted as n_P, of principal static load cases that are necessary and sufficient for this reconstruction.

A lower complexity implies either a simple structural behavior or a simple aerodynamic loading. For example, a problem with a complexity equal to 1 corresponds to a structure responding solely in a single resonant mode. In such cases, the deformed configuration of the structure at any given time is merely a scaled version of the eigenmode; both displacements and internal forces grow simultaneously, and any response can be expressed as a function of a single coordinate. Regardless of the complexity of the aerodynamic loading, if the structure responds in only one mode, the combined Aerodynamic–Structural Complexity remains equal to 1.

As another example, consider the (perhaps highly academic) scenario of a complex structure loaded at a single point in space, such as a large billboard mounted on a complex truss structure where aerodynamic loading is significant only on the billboard. In such cases, and assuming the structure responds quasi-statically, the deformed configuration at any time is a scaled version of the configuration obtained with a static analysis and a unit point load on the billboard. Therefore, regardless of the complexity of the structure in terms of geometry or diversity of material properties, the Aerodynamic-Structural Complexity remains equal to 1.

Conversely, a higher complexity indicates a problem involving complex fluid flow and structural behavior, potentially with multiple resonant modes and diverse influence lines.

Defining the Aerodynamic–Structural Complexity through the singular value decomposition of the matrix $\mathbf{F}_\mathrm{E}$ of ESWLs incorporates information about both loading and structural behavior. In a way, this extends the concept of CPT modes used as an equivalent loading (as discussed in Section 3.4.2). While CPT modes represent the principal modes of the aerodynamic loading only, PSWLs encompass the principal modes of all ESWLs, which include both the features of the aerodynamic loading and the structural response. While the former can be determined without knowledge of the structural behavior (e.g., from wind data alone), the latter is structure-specific. Therefore, it is more optimal but requires updating if, for any reason, the structural bearing system changes during the design process. Yet, the Aerodynamic–Structural Complexity is the size of the smallest space in which equivalent loads need to be described. And, to determine this, the sole analysis of the wind pressure data is not sufficient.

5 The Envelope Reconstruction Problem

5.1 Definition and mathematical formulation

The envelope reconstruction problem entails the meticulous task of identifying a sequence of static loadings $\left\{\mathbf{f}_{\mathrm{E}}^{(k)}\right\}$ that efficiently reconstruct the upper and lower envelopes, $\mathbf{z}_{\max}$ and $\mathbf{z}_{\min}$, obtained with a dynamic analysis [2, 78]. Reconstruction in this context refers to ensuring that the upper and lower envelopes of responses generated by this sequence closely approximate the actual envelopes $\mathbf{z}_{\max}$ and $\mathbf{z}_{\min}$. The envelopes generated by this sequence are determined in an iterative manner. The envelopes are initialized with the envelopes of a first static loading $\mathbf{f}_{\mathrm{E}}^{(1)}$. Then, for each additional loading the envelope is updated with the most important value among the envelope previously obtained and the one corresponding to the current static load distribution. Mathematically, for a given sequence $\left\{\mathbf{f}_{\mathrm{E}}^{(k)}\right\}$, $k = 1, \cdots, r$, the reconstructed envelope reads

$$\hat{\mathbf{z}}_{\max} = \max_{k=1,\cdots,r} \left| \mathbf{A}\mathbf{K}^{-1}\mathbf{f}_{E}^{(k)} \right| \quad ; \quad \hat{\mathbf{z}}_{\min} = \min_{k=1,\cdots,r} \left| \mathbf{A}\mathbf{K}^{-1}\mathbf{f}_{E}^{(k)} \right| \tag{5.1}$$

where $\mathbf{z}^{(k)} = \mathbf{A}\mathbf{x}_{\mathrm{E}}^{(k)}$ is the set of considered structural responses under the static loading $\mathbf{f}_{E}^{(k)}$, since we have defined the equivalent structural displacement $\mathbf{x}_{\mathrm{E}}^{(k)}$ as $\mathbf{K}\mathbf{x}_{\mathrm{E}}^{(k)} = \mathbf{f}_{E}^{(k)}$. The envelope reconstruction problem involves identifying the sequence $\left\{\mathbf{f}_{\mathrm{E}}^{(k)}\right\}$, $k = 1, \cdots, r$ which, for a given number r of static load distributions, minimizes the cost function $\psi_r\left(\hat{\mathbf{z}}_{\max} - \mathbf{z}_{\max}, \hat{\mathbf{z}}_{\min} - \mathbf{z}_{\min}\right)$, representing the disparity between the actual envelope and the envelope reconstructed with a sequence of r static loads. While a straightforward choice for ψ_r could be

$$\psi_r = \left\|\hat{\mathbf{z}}_{\max} - \mathbf{z}_{\max}\right\|^2 + \left\|\hat{\mathbf{z}}_{\min} - \mathbf{z}_{\min}\right\|^2, \tag{5.2}$$

it proves to be inefficient due to several factors. Firstly, it fails to account for structural responses with differing units (e.g., displacements and bending moments), lacking unit consistency. Secondly, it may necessitate a more nuanced definition in cases where responses in certain elements are less critical, given their over-strength. The concept of over-strength (the ratio of actual strength to design envelope value) thus emerges as a pertinent factor in constructing an appropriate cost function. Notably, during the literature review for this study, examples considering strength or capacity were scarce, indicating a potential avenue for future research.

It is crucial to acknowledge that, in most instances, the actual envelopes $\mathbf{z}_{\max}$ and $\mathbf{z}_{\min}$ for all potential responses cannot be precisely replicated using static wind loadings, as illustrated in Section 6. For the design to be on the safe side, it is important to constrain the optimization problem with two sets of inequalities

$$\hat{\mathbf{z}}_{\min,i} \leq \mathbf{z}_{\min,i} \quad ; \quad \mathbf{z}_{\max,i} \leq \hat{\mathbf{z}}_{\max,i} \tag{5.3}$$

for $i = 1, \cdots, n_{\mathrm{z}}$. On the opposite, considering the demand/capacity ratio, a controlled under-estimation may be acceptable, acknowledging that the reconstructed envelopes may not entirely encompass the actual ones [2, 78]. Moreover, it is essential to ensure that the reconstructed envelopes do not excessively overestimate the actual responses, as this would lead to uneconomical design decisions [198]. These considerations collectively underscore the challenging nature of this meticulous task, particularly for structures with significant Aerodynamic–Structural Complexity.

Although they share a common foundation (the envelopes), the determination of ESWLs and the envelope reconstruction problem represent distinct challenges, with the latter potentially addressed using ESWLs. While various mathematical formulations have been proposed for the envelope reconstruction problem, one such formulation is presented in [2], yet the concept of Universal Wind Loading was initially conceived to address both problems concurrently [39]. Subsequently, methods based on constrained least square fitting have also targeted the envelope reconstruction problem [199, 200].

Likewise, earlier works aimed at providing wind load distributions representing multiple targets in one go have undoubtedly contributed to the envelope reconstruction problem [201, 202, 203, 204], even if the problem wasn't explicitly framed as a sequence of static loading reproducing the same envelope. The same holds true for methods based on grouping responses [83, 84, 205].

5.2 Choice of the sequence

5.2.1 Based on an engineered selection of ESWLs

The various types of Equivalent Static Wind Loads (ESWLs) discussed in Section 3, especially those which enjoy the non-overshooting condition, emerge as strong contenders for inclusion in the sequence of static wind loads aimed at reconstructing the envelope, as they preclude any overestimation. Consequently, the actual envelope of structural responses can be accurately reproduced as more of such ESWLs are included in the sequence, $\lim_{r\to+\infty} \psi_r = 0$, with ψ_r as defined in (5.2). This property doesn't hold if the sequence contains ESWLs which don't satisfy the non-overshooting condition.

Within the reconstruction sequence, the upper and lower envelopes gradually take shape through the consideration of appropriate scaling factors for each ESWL (positive and negative alternately). The pace of reconstruction, termed the reconstruction rate, dictates how swiftly the actual envelope is reconstructed. The quality of convergence hinges upon the Aerodynamic–Structural Complexity of the structure since the envelope is more easily reconstructed for structures with small complexity. Also, for a given structure and wind loading scenario, a fast convergence depends on the judicious selection of structural responses. In practice, the design engineer may be tasked with identifying a set of representative structural elements, see e.g. [188]. These elements serve as the basis for reconstructing an envelope deemed sufficiently accurate for design purposes. A viable approach to achieve this accuracy entails selecting a mix of global responses (i.e., with influence lines distributed across the structure) as well as locally governed structural responses. However, the subjective nature of the process for selecting major structural responses poses a potential challenge to this method, especially for more complex structures and wind flows.

5.2.2 Based on an automated selection of ESWLs

When the selection of relevant responses is not obvious, or when there are some doubts about the subjective method described just above, it is interesting to establish an automatic procedure. A simple algorithm is presented in Algorithm 1. It is greedy but the convergence is ensured again if the ESWLs that are used enjoy the non-overshooting condition. At each iteration the sequence of static loadings $\left\{\mathbf{f}_{\mathrm{E}}^{(k)}\right\}$ is complemented with the ESWL associated with the response that is currently being the worst represented. Again, this requires the proper scaling of the responses in order to make the reconstruction process insensitive to the choice of units. It is evident that this method offers a better convergence rate as soon as the scaling used to determine the worst reproduced response is the same as that used to define the cost function ψ_r. For this reason, it will be termed "Fastest Descent" in the illustration of Section 6. Beside being locally optimum (at each iteration) in the sense of the norm of the cost function ψ_r, it prevents the structural engineer's subjective selection not to inadvertently overlook a case of fundamental importance to the design of the structure.

Algorithm 1: Automated Envelope Reconstruction Algorithm based on ESWLs (Fastest Descent)

```
Initialize reconstructed envelope, ẑ_max ← 0, ẑ_min ← 0
Initialize empty loading sequence, {f_E^(k)} ← {}, r ← 0
Pick a response of interest (user-defined), or select a response randomly
while not_reconstructed_yet do
    Calculate responses associated with current wind load, z^k_max, z^k_min
    Update reconstructed envelope, ẑ_max ← max(ẑ_max, z^k_max), ẑ_min ← min(ẑ_min, z^k_min)
    Find the response with the biggest discrepancy
    Select ESWL associated with worst response
    Add selected ESWL to loading sequence
    Check if desired reconstruction accuracy is reached, update not_reconstructed_yet
```

5.2.3 Based on PSWL and Aerodynamic-Structural Complexity

Considering that multiple responses can be targeted simultaneously, see e.g. [204], one might consider building the sequence of reconstructing static loadings $\left\{\mathbf{f}_\mathrm{E}^{(k)}\right\}$ using distributions other than just the Equivalent Static Wind Loads (ESWLs) associated with individual responses. Principal Static Wind Loads (PSWLs) emerge as promising candidates due to their inherent definition. Indeed, the first PSWL derived from a comprehensive set of ESWLs reflects the distribution of loads on the structure that best replicates the most common ESWLs. So if only one static load would have to be selected to reproduce as much as possible from the whole envelope, it is expected that it would be the first PSWL. As illustrated in Section 6 too, we shall warn, however, about a blind application of PSWLs as a sequence of reconstructing static loadings $\left\{\mathbf{f}_\mathrm{E}^{(k)}\right\}$.

Since PSWLs result from an eigenvalue decomposition, they require a scaling similar to the method discussed in Section 3.3.1, concerning the Equivalence condition. Specifically, they can be normalized such that the corresponding envelope is tangent to the envelope being reconstructed (tangency condition, see e.g., [111]). Yet, due to this necessary rescaling, not all PSWLs are guaranteed to be tangent to the actual envelope at various points. This is in contrast to the set of all ESWLs, provided they all satisfy the non-overshooting condition, as each of them reconstructs the envelope for a distinct value. Consequently, this leads to the observation that $\psi_r^+ \not\to 0$ as $r \to +\infty$ when the sequence $\left\{\mathbf{f}_\mathrm{E}^{(k)}\right\}$ is created using PSWLs.

However, it is reasonable to anticipate that utilizing the first (few) n_P PSWLs yields a faster reproduction of the actual envelope compared to the same number n_P of ESWLs, especially when n_P is small. This arises from the ability of PSWLs to capture multiple ESWLs (responses) simultaneously. The optimal value of n_P for achieving this performance depends on the Aerodynamic–Structural Complexity. This is illustrated in Section 6 but this statement is understandable in a more general context, just by considering limiting cases. For a structure with complexity 1, e.g. a light-pole responding in a single mode, it is clear that the actual envelope can be reconstructed with only one loading mode: all ESWLs are (almost) identical and the first PSWL is very similar too. As complexity grows the first few PSWLs tend to not perfectly reproduce the envelope, since the tangency condition is not satisfied at significantly different abscissa. A rule-of-thumb recommendation would be to choose n_{P} equal to or of the same order of magnitude as the Aerodynamic–Structural Complexity.

For this moderate number of PSWLs, one should not expect the actual envelope to be accurately reconstructed. The remaining "gaps" can be addressed through a second distinct phase, which involves supplementing the sequence $\left\{\mathbf{f}_{\mathrm{E}}^{(k)}\right\}$ with additional load distributions. At this juncture, the most favorable approach is to employ for this second phase a steepest descent method, as discussed in Section 5.2.2, as it is optimal for filling these remaining gaps.

5.2.4 Based on combinations of PSWL

Alternatively, it is possible to opt for a reconstruction of the envelope based on combinations of PSWLs. This approach somehow generalizes the solution described in the previous Section in the sense that (i) to choose the first few PSWLs in the first phase is just a particular case of combinations (with only one non-zero combination coefficient at time), (ii) the ESWLs chosen to finalize the process with the steepest descent are also combinations of PSWLs. So the sequence presented in Section 5.2.3 can be seen as being constructed with combinations of PSWLs at each stage of the process.

To make it more efficient, it is possible to develop a steepest descent such as described in Algorithm 1 from the beginning of the construction of the sequence. At each iteration the best combination of PSWLs would be used instead of (i) just one PSWL (for the first few loadings), then (ii) the best ESWLs (to refine with the steepest method).

From a pragmatical stand point, the design engineer should keep a limited number of PSWLs. Remembering that the Aerodynamic–Structural Complexity is defined as the number n_{C} of PSWLs such that any ESWL can be recombined from the first n_{C} PSWLs with a small controlled discrepancy, each step of the algorithm consists in determining the best n_{C} combination coefficients that optimize the reconstruction rate of the envelope. This task is constrained by the non-overshooting condition of the envelope, and the tangency condition is managed in the same way as explained earlier. This constrained optimization problem can be efficiently solved with existing algorithms based on Lagrange multipliers [206], genetic algorithms [207], differential evolution [208], or with more traditional approaches such as the sequential linear programming algorithm, the (modified) method of feasible directions algorithm, and the sequential quadratic programming, differential evolution [209].

It is also to be mentioned that ESWLs can be combined to reproduce the envelope [210], a process which follows closely the spirit of PSWLs. However, using the original basis of ESWLs to reconstruct the envelope with an automatic search procedure is more time-consuming than to work in the low-dimensional space spanned by the PSWLs.

5.3 Overestimation, underestimation

From this earlier discussion, it is evident that the non-overshooting condition plays a major role in tackling the envelope reconstruction issue. Overshooting arises when an Equivalent Static Wind Load generates responses in the structure exceeding the actual envelope. In such instances, a couple of choices emerge: either scale down the ESWL to meet again the tangency condition or retain the ESWL unchanged, albeit resulting in an overestimation of the reconstructed envelope. Opting for the former does not ensure that all responses can still be accurately reconstructed with the set of ESWLs, much like the challenges encountered with PSWLs, as discussed in Section 5.2.3. Consequently, the allure of the second solution grows, yet accurately predicting the extent of overestimation beforehand proves challenging, if not impossible.

Hence, it should be recommended to employ ESWLs satisfying the non-overshooting condition whenever feasible. This is not necessarily possible when peak factors of structural responses differ across responses or when responses exhibit non-Gaussian behavior, aspects left unexplored in the previous Sections.

Another crucial aspect to consider is the potential for underestimating the reconstructed envelope, offering flexibility to enhance or streamline the reconstruction process. This involves setting the envelope to be reconstructed at a fraction, say 95%, of the actual envelope. By employing this approach, the reconstruction sequence can be terminated earlier, thereby limiting the number of loadings required for envelope reconstruction.

For a more comprehensive understanding of over- and under-estimation, a detailed discussion is provided in [78], along with illustrative examples. Achieving the right balance between over- and under-estimation of the envelope entails finding case-specific trade-offs in the total number of loadings necessary for envelope reproduction. It is also noticed that the definition of over- and under-estimations should involve dialogue with project managers as well.

5.4 Management of the average response

In the preceding discussions, the average response was deliberately omitted due to specific simplifications made for clarity. We had left aside the average wind loading and the average structural responses.

Since ESWLs are derived from a straightforward linear structural analysis, the superposition principle applies. Consequently, in all previously examined scenarios where the average response was absent, incorporating it involves simply adding the average wind loading to the ESWLs, thereby reconstructing the upper and lower envelopes adjusted by the mean value. On a side note it is noted that when applying the tangency condition, the normalization factor λ is to be applied solely to the fluctuation around the mean value, not on the mean loading.

5.5 Non-symmetric (non Gaussian) envelopes, nonlinear responses

Once the mean response is incorporated, the actual upper and lower envelopes differ in absolute value. However, as discussed previously, this disparity does not impede the application of the methods discussed earlier. Therefore, a minor incongruity between the upper and lower envelopes should not pose a significant obstacle in resolving the envelope reconstruction problem.

There are essentially two approaches to address non-symmetric envelopes, reflecting the non-Gaussian nature of the responses for instance because of (i) a nonlinear memoryless transformation of structural coordinates to responses, (ii) a nonlinear structural behavior, (iii) a non-Gaussian response to a non-Gaussian wind loading. The first approach involves working with two distinct envelopes, one upper and one lower, potentially disparate, and reconstructing them using different load cases. The second approach entails computing the mean envelope $\frac{1}{2}\left(\mathbf{z}_{\max}+\mathbf{z}_{\min}\right)$, which no longer equals zero, and assigning a static load case to it. This static load case can be added to the average wind loading or handled similarly, rendering the virtual envelope to be reconstructed symmetric.

Regardless of the chosen method, relying on standard ESWLs does not ensure adherence to the non-overshooting condition. The LRC method, upon which standard ESWLs are based, assumes Gaussian response. Consequently, standard ESWLs might not provide a robust foundation for PSWLs which are necessary for envelope reconstruction. Given this flexibility, alternative approaches are conceivable, motivating the development of the Displacement-Response Method (see § 3.8). Particularly, the utilization of a cubic translation model to define ESWLs as the most probable loads conditioned on a known response has been explored. Specifically, we introduced the bicubic translation model [3], a formulation capable of providing a closed-form expression for the conditional mean of structural displacements given a known response. This model remains valid in a non-Gaussian framework and converges to the established Gaussian formulation when skewness and kurtosis vanish, asymptotically. While this method yields realistic wind load distributions, like others, it cannot guarantee adherence to the non-overshooting condition. In scenarios involving non-Gaussian structural responses or even just non-Gaussian wind loads, it is advisable to relax the envelope reconstruction problem by tolerating some over- and under-estimations of the actual envelope.

5.6 Objectives, technical/logistic constraints

Equivalent and Principal Static Wind Loads serve as tools to facilitate communication between structural and wind engineers, particularly in addressing the envelope reconstruction problem. Despite the increasing accessibility of dynamic step-by-step analysis for many structural engineers, the necessity of static equivalent loads remains pertinent. This is especially true when dealing with numerous load combinations, which could pose challenges if each one needs to be individually considered.

The primary objective of simplifying communication between structural and wind engineers can only be realized if the exchange of information remains concise and easy to process. On one hand, constructing Equivalent Static Wind Loads requires structural matrices ($\mathbf{M}$, $\mathbf{C}$, $\mathbf{K}$), along with the geometric positions of pressure taps and tributary areas. On the other hand, once the envelope reconstruction problem is solved, the sequence of static forces needs to be transmitted back, regardless of the adopted solution.

The method based on PSWLs is particularly appealing, as it involves providing a limited set of load cases (the PSWLs) along with combination coefficients. Structural engineers are accustomed to combining loads, making this approach highly practical. While the other options based on a set of independent ESWLs are available, they necessitate a number of independent load cases, and not load combinations of a small number of load cases. Therefore, working with a few PSWLs and combining them simplifies the process and reduces the likelihood of human error, as there is also less information to manage and transmit.

The proposed algorithm faces technological challenges, particularly regarding memory limitations associated with establishing all ESWLs and performing the singular value decomposition (4.2) required for the determination of PSWLs. However, recent advancements in computational methods, such as online techniques for singular value decomposition [211], have mitigated these concerns, making memory limitations less significant. For instance, an interesting alternative to explore is to compute PSWLs sequentially, starting from a limited set of ESWLs and refining their values as additional ESWLs are included. This sequential approach offers a more efficient use of memory storage and computational resources.

Considering these factors, solutions based on combinations of PSWLs, as discussed in Section 5.2.4, appear highly appealing. These PSWLs can be derived from any of the ESWL approaches outlined in Section 3, whenever applicable, highlighting the flexibility of the methodology.

6 Illustration

6.1 The considered problem

To illustrate the various methods presented in the preceding Sections, we employ an academic example of a seven-span bridge. The spans are chosen equal to 300 m, except for the last span, slightly longer (305m), in order to exacerbate the asymmetry in the mode shapes. This example is intentionally straightforward, making it easily reproducible for users. All Matlab routines used to develop this academic example are available [1]. Yet it exhibits a sufficient level of structural complexity for distinguishing between the different methods. For instance, not all influence lines of the studied responses exhibit constant signs, indicating that methods based on the gust response factor would not be suitable.

The structure is modeled using a finite element beam model, where the beams have a flexural stiffness $EI = 10^{10}$ kN.m^2 and a mass per unit length μ =10 tons/m. The model counts 12 elements per span, a total of 85 nodes at which 2 degrees–of-freedom (DOFs) are used: transverse displacement and rotation. Stiffness and mass matrices are constructed with standard Finite Element (FE) methods [7]. A modal damping $\xi = 0.3\%$ in each mode is imposed. Figure 6.1 gives a picture of the first 8 modes shapes and highlights the high spectral density, with the first 7 modes ranging from 0.55 Hz to 1.20 Hz.

The aerodynamic loading on this structure follows a simplified version of Eurocode rules, considering only the longitudinal component of turbulence for simplicity, and accounting for drag forces exclusively. The aerodynamic loading is constructed with $v_{b,0} = 24$ m/s in category terrain II, and at a height ($z = 100$ m) of the deck $U = 34.7$ m/s, $\sigma_u = 4.56$ m/s. With a deck width $B = 30$ m and a drag coefficient $C_D = 0.4$ under mean incidence, this results in an average wind load of 8.794 kN/m. The cross-power spectral density of the longitudinal turbulence follows

$$S_{u_1 u_2}(f;\Delta x) = 4\frac{L_{ux}}{U}\sigma_u^2 \frac{\mathrm{e}^{-C\frac{f\Delta x}{U}}}{\left(1+70.7\left(f\frac{L_{ux}}{U}\right)^2\right)^{5/6}} \tag{6.1}$$

where Δx is the distance between the two consider points. It is expressed as a function of frequency and such that the integral of unilateral PSDs over frequency f on $[0, +\infty]$ returns the variance. The turbulence lengthscale is chosen as $L_{ux} = 50$ m and space coherence is modeled as a real decreasing exponential with constant $C = 8$. The cross-section admittance and aerodynamic damping are neglected [5]. The simplest formulation for the aerodynamic buffeting load [5] is finally

$$p\left(x,t\right) = \frac{1}{2}\rho C_D B U^2 + \rho C_D B U u\left(x,t\right). \tag{6.2}$$

The loading is a linear transformation of the Gaussian turbulence field $u\left(x,t\right)$. It can be recovered as a particular case of more general buffeting loading models [212, 213]. With the chosen numerical values, the standard deviation of the fluctuation of wind loads is equal to 2.31 kN/m. Table 1 summarizes the numerical values chosen in this illustration.

Samples of the wind loads at the nodes of the finite element model are generated to mimic a typical scenario where a structural engineer has an available finite element model, and a wind engineer determines a pressure field (or force distribution) on the main structural elements. These samples are generated using the spectral decomposition of the cross Power Spectral Density (PSD) [214]. The time step is set to $\Delta t = 0.04$ s, and the total duration is $T_{\mathrm{sim}} = 2621$ s (65536 time steps). This duration is slightly longer than conventional stationary windows but allows for better statistical estimators in a simulation context.

[1] Reference to repository will be made available if paper is accepted for publication

Average wind velocity	$U = 34.7$ m/s	Deck width	$B = 30$ m
Turbulence intensity	$I_u = 13.2\%$	Drag coefficient	$C_D = 0.4$
Turbulence lengthscale	$L_{ux} = 50$ m	Bending stiffness	$EI = 10^{10}$ kN.m^2
Space coherence coefficient	$C = 8$	Mass per unit length	$\mu = 10$ tons/m

Tab. 1: Numerical values chosen for the illustration

	Mode 1	Mode 2	Mode 3	Mode 4	Mode 5	Mode 6	Mode 7
σ_q	0.0235	0.0242	0.0172	0.0114	0.0081	0.0058	0.0050
$\sigma_{q,\mathrm{R}}$	0.0228	0.0235	0.0166	0.0109	0.0076	0.0054	0.0045
$\sigma_{q,\mathrm{B}}$	0.0057	0.0061	0.0047	0.0034	0.0027	0.0021	0.0022

Tab. 2: Standard deviations of modal responses (in m): total response σ_q and split-up into the background ($\sigma_{q,\mathrm{B}}$) and resonant ($\sigma_{q,\mathrm{R}}$) contributions.

With only these time series and the finite element model available, structural analysis is conducted using a time marching algorithm [7]. For this example, only fluctuations around the mean loading are retained, by dropping the first term in (6.2). The analysis is carried out in the modal basis to obtain the time evolution $\mathbf{q}(t)$ of fluctuations of modal coordinates around their mean. The standard deviation of modal coordinates is then determined (see Table 2). The quasi-static component of the response is obtained using a quasi-static calculation involving the covariance matrix of forces [92]. The quasi-static variance is subtracted from the total variance to obtain the variance of the resonance component for each mode.

For illustration, the time series of some structural responses can be determined. As examples, the displacements at midspan in the 2nd, 4th, and 6th spans are shown in Figure 6.2. This figure illustrates that the response is mostly resonant. The Power Spectral Densities (PSDs) are estimated via periodograms of the time series, explaining the erratic character of the power spectral densities. In parallel, a spectral analysis in the frequency domain, with the smooth analytical expressions of turbulence PSD, has been carried out. With a fine meshing of the frequency space, the PSDs of structural responses were also determined. They are represented with thin dashed lines. The good agreement between these two sets of results shows the equivalence between a time domain simulation based on samples (Monte Carlo) and a probabilistic frequency domain approach.

The reconstruction of the envelope requires defining the envelope. As explained earlier, the proposed approach considers a rather broad selection of responses to ensure that an arbitrary user selection of a few responses deemed important does not bias the process of determining the design load cases. In this illustration, the relevant responses include the transverse displacements and the bending moments at each of the 85 nodes in the finite element model. Shear forces are discarded, and axial forces are trivially null, leaving a total of 170 responses.

Furthermore, to better highlight the importance of the non-overshooting property, the peak factors are discarded from the analysis. This ensures that the envelope of responses simply coincides with their standard deviations. In a more realistic context, the final design could be carried out by applying unique peak factors on these results.

6.2 ESWLs and PSWLs

Figure 6.3 shows three ESWLs obtained through the LRC method. These loads are designed to reconstruct midspan displacements in the 2nd, 4th, and 6th spans. The lower part of the figure displays the ESWLs, while the upper part illustrates the corresponding displacements. The ESWLs have been rescaled to ensure that the responses are effectively tangent to the envelope, which is

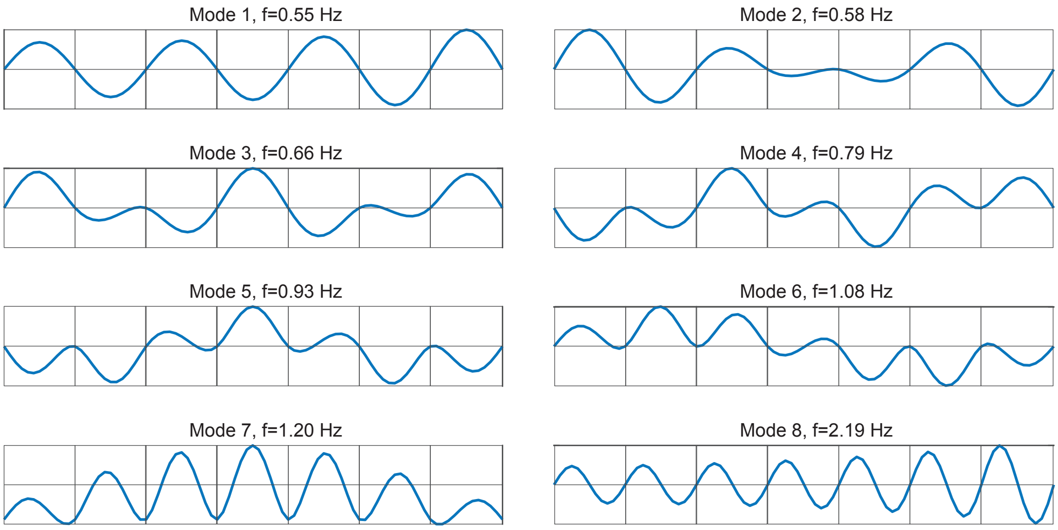

Fig. 6.1: Eigen modes and natural frequencies (in Hz).

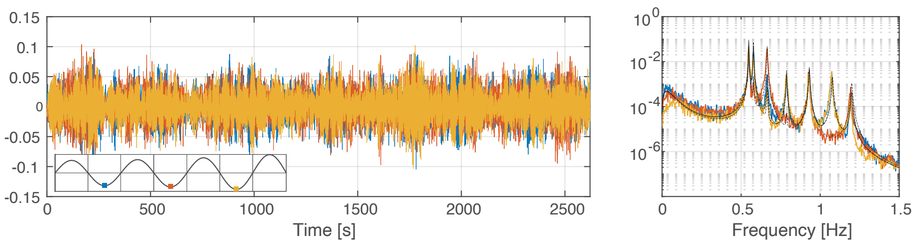

Fig. 6.2: Examples of displacements at mid-span in 2nd, 4th and 6th spans (time series and corresponding PSDs).

depicted in light gray in the background. The envelope is also symmetrically represented ($\pm\sigma_z$) as a Gaussian response is expected here.

While the displacements obtained under these three load cases appear to be contained within the response envelope, it is noted that this observation is specific to the chosen case and the three selected responses. If the representation had been for displacements closer to the support, minor overestimation might have occurred. This stems from the quasi-static assumption in the LRC approach and the predominance of resonance in this example.

In Figure 6.3, the solid lines represent the LRC load distributions and the corresponding displacements obtained using sampled time series (Monte Carlo). In this case, covariances between applied loads and structural responses are determined through (2.8) and statistics over time series. The thin dashed lines depict the same quantities but obtained through spectral analysis in the frequency domain, resulting in a much smoother outcome, as anticipated. It is important to note that these two results have been obtained through two independent simulations, sharing only the same information about the FE model and wind loading.

For the first two responses, i.e., displacement in the midspan of the 2nd and 4th spans, the two approaches align well. While the ESWL might differ slightly, the structural responses are very similar. However, the responses generated under the ESWL corresponding to the displacement in the 6th span differ significantly, especially in the 4th and 5th spans (see yellow line). This discrepancy arises from two distinct load distributions under the two methods. In particular, the frequency domain approach localizes the ESWL in the three rightmost spans (thin dashed yellow line), whereas the LRC load distributions obtained with the Monte Carlo approach still suggest significant values in the left half of the structure. This illustrates the limitations of the Conditional Sampling Technique, the sample-based version of the LRC. To enhance its effectiveness, a substantially larger number of samples in the time series (much more than 2^{13}) would be necessary, even though they have been sampled with a relatively large time step here to alleviate the issue.

The alternative of using CPT modes as Equivalent Static Wind Loads is illustrated in Figure 6.4. The fifth CPT mode is represented by the solid blue line in the bottom part of the figure. It exhibits symmetry with respect to the half length of the model (2105m $\div$ 2) as it is derived from the homogeneous wind field. However, the response of the non-symmetric bridge (due to the 7th span being slightly longer) results in a visibly non-symmetric response. Scaling is necessary for CPT modes as they result from an eigenvalue problem, see Section 3.4.2. The scaling is again performed following the equivalence condition, to recover the displacement in the second span, as indicated by the short arrow.

In this case, the overshooting of the actual envelope exceeds 10%. Consequently, while this CPT mode could be considered as an ESWL, it would be necessary to reconsider the scaling to find a balance between the overshooting of the envelope and the reconstruction of the desired response. The situation is even more challenging with the third CPT mode, depicted in dashed grey. The magnitude of this load distribution needs to be much larger ($\sim$500kN at nodes of the FE model) to generate the desired displacement in the second span. This is accompanied by significant and likely unacceptable overshooting in the side spans and in the middle span.

Although not illustrated here, the 7th CPT mode is found to be rather accurate in reconstructing the response envelope. This accuracy is attributed to the nearly periodic feature of the problem and the alignment of this mode with the Modal Inertial Load (MIL) in the fundamental mode. In more general problems, it is improbable that they correspond, as one is based on the covariance matrix of the loading and the other on the balance of inertial and elastic restoring forces in the structural system.

Last but not least, if the 1st CPT mode were used to reconstruct responses (depicted by green dashed lines), the load distribution would closely resemble the mean wind loading, without changing sign along the entire bridge. The displacements would then mirror the deformations of

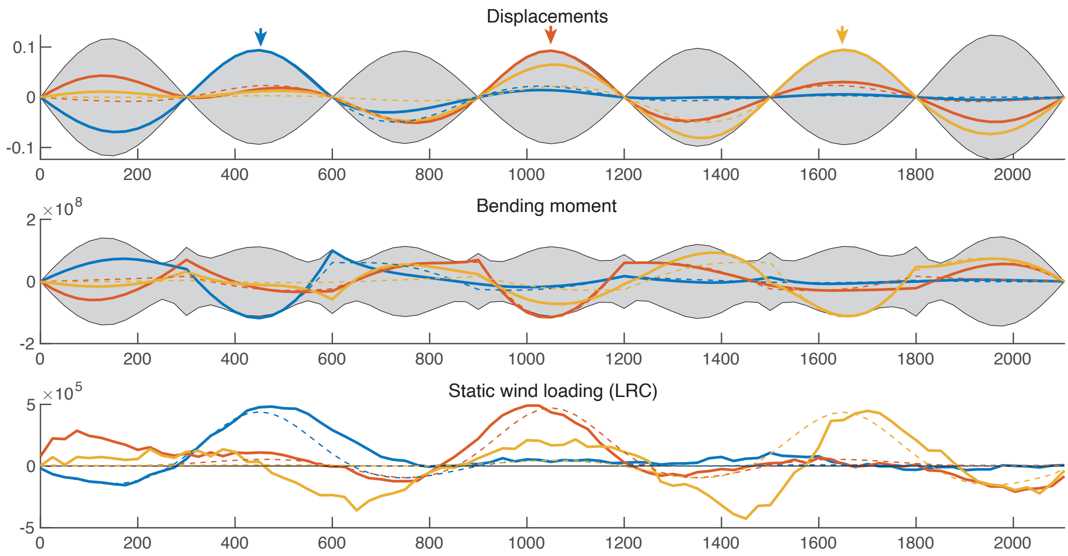

Fig. 6.3: Illustration of the LRC method. Bottom: equivalent static wind loads corresponding to displacements at midspan in 2nd (blue), 4th (red) and 6th (yellow) spans. Top: the corresponding deformed configurations (in m) and bending moment diagrams (in Nm). Scaling has been applied to recover the actual response. The solid lines correspond to the results obtained with the sampled wind loads while thin dashed lines correspond to application of a spectral analysis.

the structure under a uniform loading. However, in this case, it is observed that applying scaling to recover the displacement in the 2nd span leads to significant overestimations in the rest of the structure. This highlights the well-known principle that the usage of the Gust Response Factor should be limited to cases where the influence lines do not change sign.

Figure 6.5 shows the ESWLs obtained as a weighted combination of LRC distributions and MILs, with (3.24). Three load distributions are represented in the bottom line of the Figure. They aims at reproducing, respectively, the maximum displacements in the middle of the 2nd (blue), 4th (red) and 6th (yellow) spans. Modal correlations can be estimated with a background/resonant decomposition [13] and are sufficiently small in this problem to be neglected. A simplified version, assuming $\rho_{q,ij} = \delta_{ij}$, of the more general method [95] presented in Section 3.7 is implemented. Since the responses are mostly resonant, the weighting of the MIL dominates the LRC and the resulting ESWLs naturally appear smoother. It is observed that the responses, in terms of displacements and bending moments, obtained under these three loads cases all fit within the envelope. This is because this method enjoys the non-overshooting property. Furthermore, it is observed that the ESWL reproducing the maximum displacement in the second span (in blue) also reconstructs the maximum bending moment in the same span. This is explained by the fact that (i) they have similar influence lines (LRC part), (ii) a vibration mode having a sinusoidal form has maximum displacement and maximum bending moment (second derivative) at mid-span (MIL part). Application of the load case with opposite sign generates the responses indicated with a thin line in Figure 6.5. Considering both the positive and negative load cases, and these three distributions, it is observed that the envelope is partly reconstructed: bending moments and displacements are accurately represented in the 2nd, 4th and 6th span; they are only partly represented in odd rank spans, and bending moments on supports are poorly reproduced. This will be further discussed in

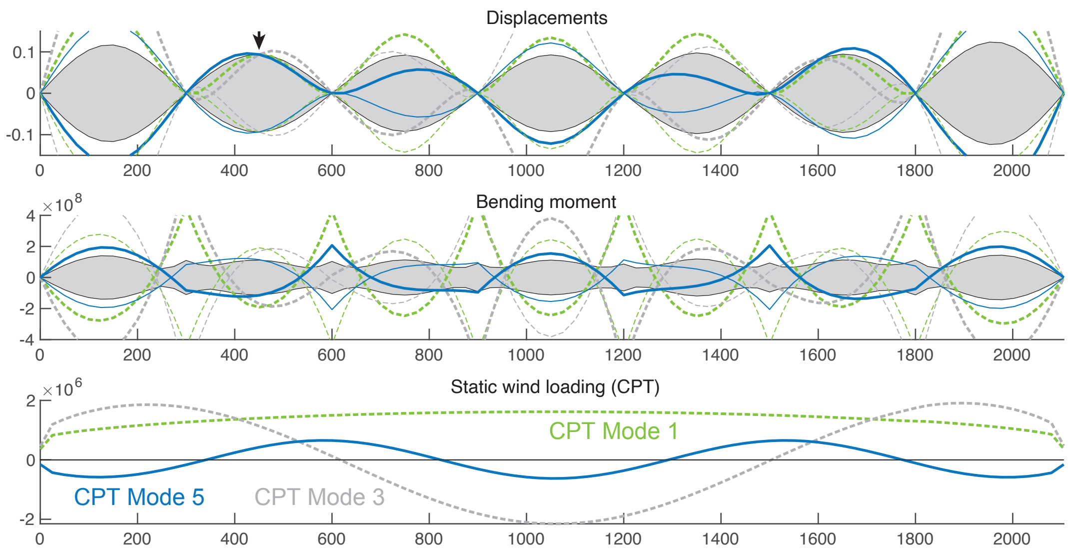

Fig. 6.4: Illustration of the CPT modes. Bottom: equivalent static wind loads corresponding to displacements at midspan in 2nd span for CPT mode 5 (blue) and CPT mode 3 (grey). Top: the corresponding deformed configurations (in m) and bending moment diagrams (in Nm). Scaling has been applied to recover the actual response. Minor overshooting (mode 5) and significant overshooting (mode 3) are observed.

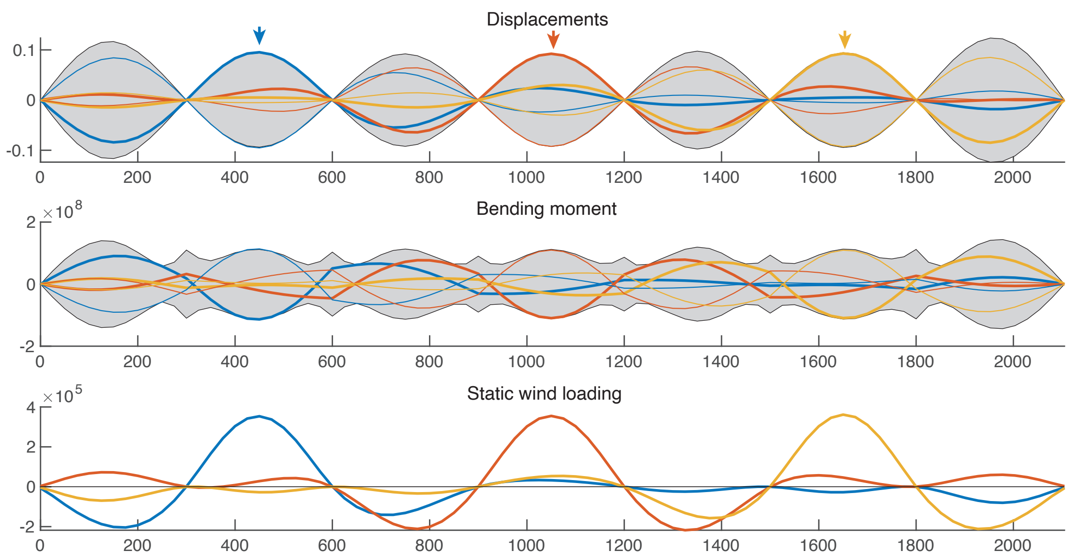

Fig. 6.5: Illustration of ESWL obtained as a weighted combination of LRC distributions and MILs. Bottom: equivalent static wind loads corresponding to displacements at midspan in 2nd (blue), 4th (red) and 6th (yellow) spans. Top: the corresponding deformed configurations and bending moments. Scaling is not necessary.

the section devoted to envelope reconstruction.

The three ESWLs shown in Figure 6.5 are just 3 examples of ESWLs that could be imagined for this structure. In fact, such a load distribution exist for each and every considered displacement in the finite element model. Considering here transverse displacements only at the 85 nodes of the model, a collection of 85 ESWLs can be established. It is represented in Figure 6.6 by means of contours. We can examine a detailed example to better interpret this diagram. Numbering nodes from 1 to 85, starting on the left end of the bridge, the ESWL reconstructing the displacement in the middle of the second span is numbered 19. On Figure 6.6, at level 19, the ESWL is negative in the 1st and 3rd spans, positive in the second, and is negligible in the remaining spans. This represents the distribution shown in blue in Figure 6.5. The operation can be realized with bending moments too. Results are shown on the right in Figure 6.6. The pattern is similar for bending moments, especially at midspan, which are maximized when loads are alternating signs on adjacent spans.

The two 85×85 matrices shown in Figure 6.6 are placed on top of each other to create a bigger matrix (170×85) collecting the 170 responses on lines and the 85 loading nodes along columns. This is the most compact, static, information, relating loads and responses. This collection of 170 load distributions can be seen as a collection of 170 vectors in an 85-dimensional space. The SVD decomposition of this matrix seeks the directions in that space which are shared by these vectors, and sorts them from most to worst relevant. The corresponding loading modes are the Principal Static Wind Loads (PSWL). Each and every PSWL comes with a singular value, quantifying its relevance in the collection of ESWLs. The first 7 PSWLs and the corresponding singular values are represented in Figure 6.6. Although they remain relatively smooth, their shapes differ from those of the ESWLs. Lower PSWLs modes capture the essence of the most common ESWLs, while the higher PSWL modes are there to fill the gaps of the basis.

In this example, only the first 7 PSWLs have significant singular values. As a consequence the Aerodynamic–Structural Complexity of this bridge is equal to 7, meaning that any of the 170 considered structural responses can be recovered, without overshooting of the envelope, with a combination of only 7 independent PSWLs. The structural complexity is an intrinsic property of the structure and its aerodynamic loading. One would have obtained the same value by considering axial and shear forces in the responses, or by considering only one displacement out of two. The structural complexity is therefore independent of an arbitrary choice of responses that are assumed to lead the design (up to a reasonable discretization).

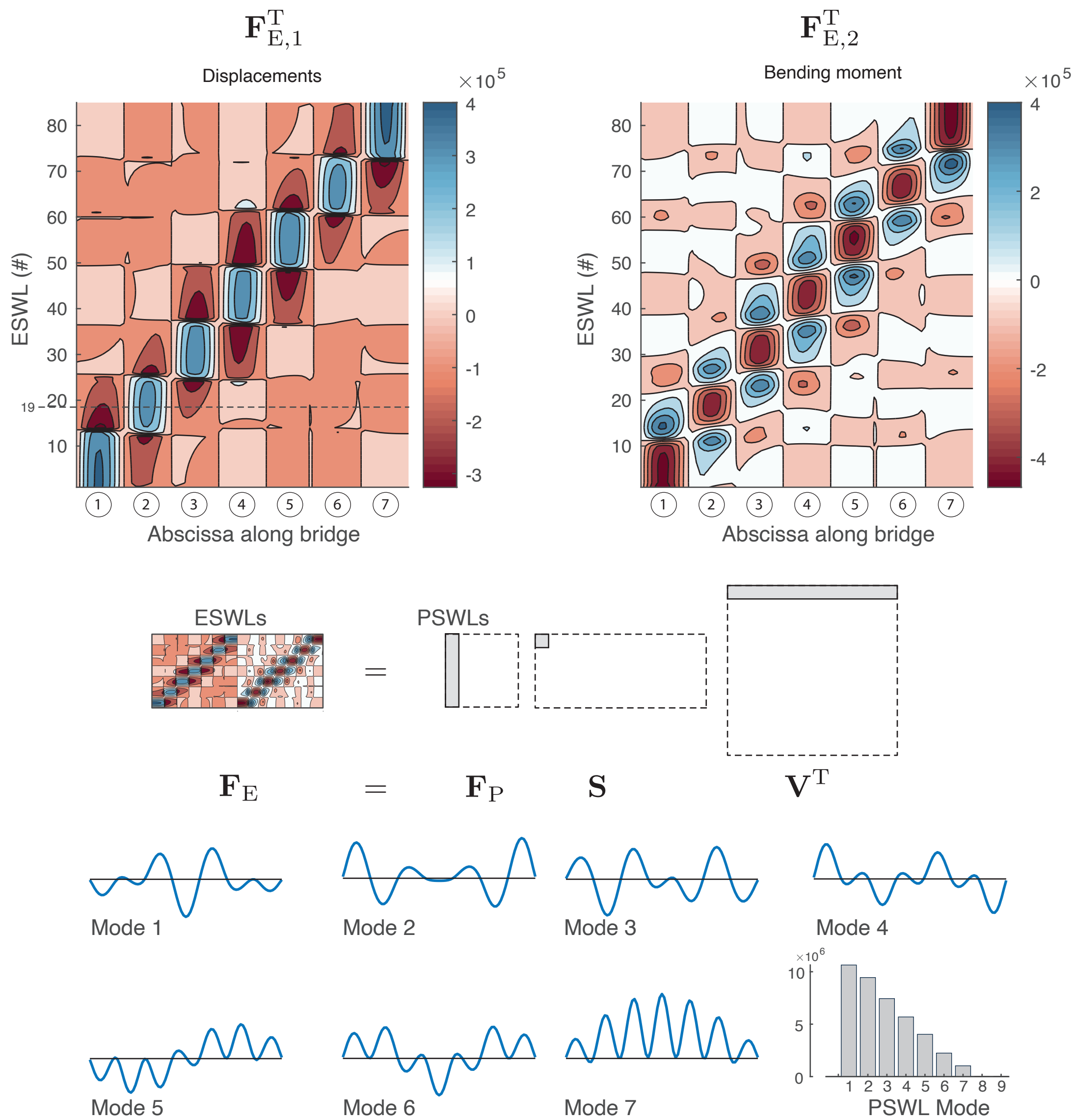

Fig. 6.6: Determination of the Principal Static Wind Loads (PSWLs). They are obtained through the singular value decomposition of the response matrix combining the ESWLs associated with all responses (in this case displacements and bending moments). Each principal mode comes with an singular values that allows ranking them from most to worst relevant. The bottom part represents the first seven PSWL. The structural complexity of this structure and its loading is seen to be equal to 7.

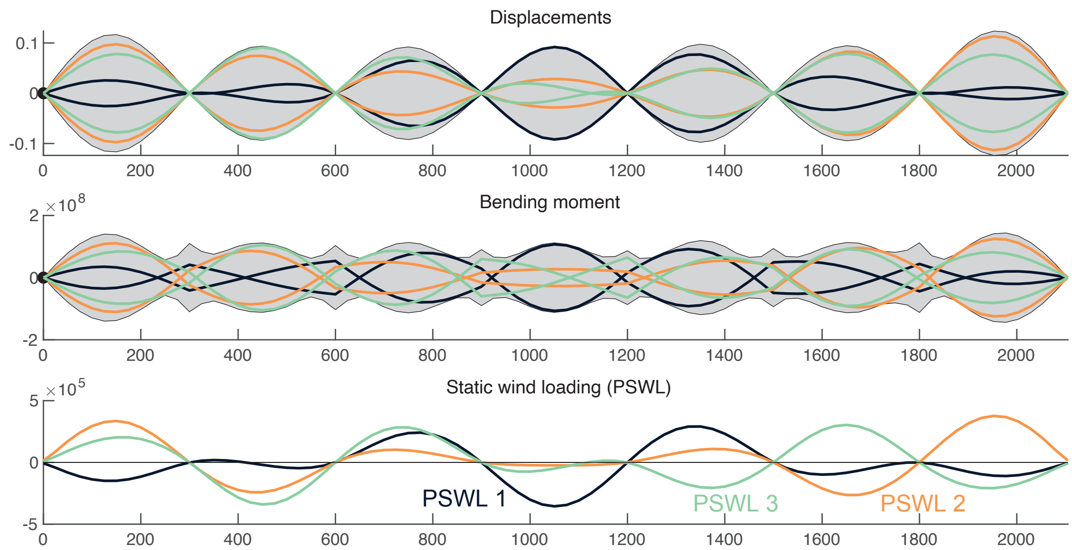

Fig. 6.7: Illustration of the first three PSWLs and their usage as ESWLs. Bottom: PSWL 1, 2 and 3. Top: the corresponding deformed configurations and bending moments. Scaling is necessary and has been applied to satisfy the tangency condition of the envelope.

6.3 Envelope reconstruction

In this Section the envelope reconstruction problem is solved with the different options presented in Section 5.2, for the selection of the sequence of static loads. Figures 6.5 and 6.5 give a good introduction to what the envelope reconstruction problem is. In these Figures, the two upper diagrams show the displacements and bending moments in the structure, respectively under three selected ESWLs, and under the first three PSWLs. The envelopes $(\hat{\mathbf{z}}_{\min}, \hat{\mathbf{z}}_{\max})$ of the responses generated by these two sequences $\left\{\mathbf{f}_{\mathrm{E}}^{(k)}\right\}$, for $k = 1, 2, 3$ $(r = 3)$, are not represented but can be easily imagined. They approach the actual envelope $(\mathbf{z}_{\min}, \mathbf{z}_{\max})$ which is represented in light gray in the background. They do so without overshooting because one the one hand the chosen ESWLs enjoy the non-overshooting condition and, on the other hand, the PSWLs have been scaled to meet the tangency condition. In the envelope reconstruction problem, it is expected that more static loads are required to accurately reproduce the actual envelope.

Figure 6.8 illustrates this convergence for the four sequences of static loads discussed in Section 5.2. Since the envelope is symmetric $(g^+ = g^-)$, it is reconstructed by considering the same load distributions once taken positively, and once take negatively, so as to reconstruct the two envelopes at the same time. The solutions are compared with the following two indicators

$$\psi_r^{\mathrm{displ}} = \frac{\left\|\hat{\mathbf{z}}_{\max}^{\mathrm{displ}} - \mathbf{z}_{\max}^{\mathrm{displ}}\right\|^2}{\left\|\mathbf{z}_{\max}^{\mathrm{displ}}\right\|^2} \quad ; \quad \psi_r^{\mathrm{mom}} = \frac{\left\|\hat{\mathbf{z}}_{\max}^{\mathrm{mom}} - \mathbf{z}_{\max}^{\mathrm{mom}}\right\|^2}{\left\|\mathbf{z}_{\max}^{\mathrm{mom}}\right\|^2} \tag{6.3}$$

which represent the reconstruction rates of the displacements and bending moment diagram. By separating the cost function ψ_r into two, the question of unit consistency is alleviated. In a real application, the two indicators would probably be combined into a single one, e.g. $\psi_r = \frac{1}{2}\left(\psi_r^{\mathrm{displ}} + \psi_r^{\mathrm{mom}}\right)$. In this paper it is decided to keep both to provide some more insight on the separate reconstructions of each diagram.

In the naive approach with ESWLs (§ 5.2.1), some ESWLs are carefully chosen in an engineered decision. In this case, we have chosen the 7 displacements at the mid-spans followed by the bending moments on the supports. The detailed diagrams represented in the bottom part of the Figure show the progressive reconstruction of the envelope. For instance, after having considered 1 loading mode $(r = 1)$, the envelope of the displacement is well reproduced on the left, and so is the bending moment at mid-span in the first span. After consideration of the second loading mode $(r = 2)$, the displacement in the second span is now reconstructed, and this process goes on as r grows. For $r = 7$, all 7 mid-span displacements have been considered and it is seen that the envelope of displacements is almost perfectly reproduced. At the same time, the reconstructed envelope of bending moments reproduces well the actual envelope, except on supports. This explains why, for $r = 8$ and following, the sequence is extended with the ESWLs corresponding to bending moments on supports. For $r = 10$, the bending moments on the first 3 supports is well capture, and another set of 3 additional ESWLs seems necessary for a acceptable reconstruction of the envelope.

The black curves in the upper part of Figure 6.8 shows the reconstruction rates ψ_r^{displ} and ψ_r^{mom} with the sequence being considered. From ψ_r^{displ}, the envelope of displacements is seen to be monotonically reconstructed and has reached 98.1% for $r = 7$, while at the same time, the indicator ψ_r^{mom} related to bending moments is still below 90% (bending moments on supports are still inaccurately represented).

In the fastest descent approach with ESWLs (§ 5.2.2), the sequence is initialized with the reconstruction of the transverse displacement in the leftmost span. So the first iterate is the same as in the naive approach. Then, for $r \geq 2$, the worst represented response is picked and the corresponding ESWL is appended to the reconstructing sequence. In this case, for $r = 2$, the displacement in the rightmost span is picked, then for $r = 3$, the displacement in the middle span,

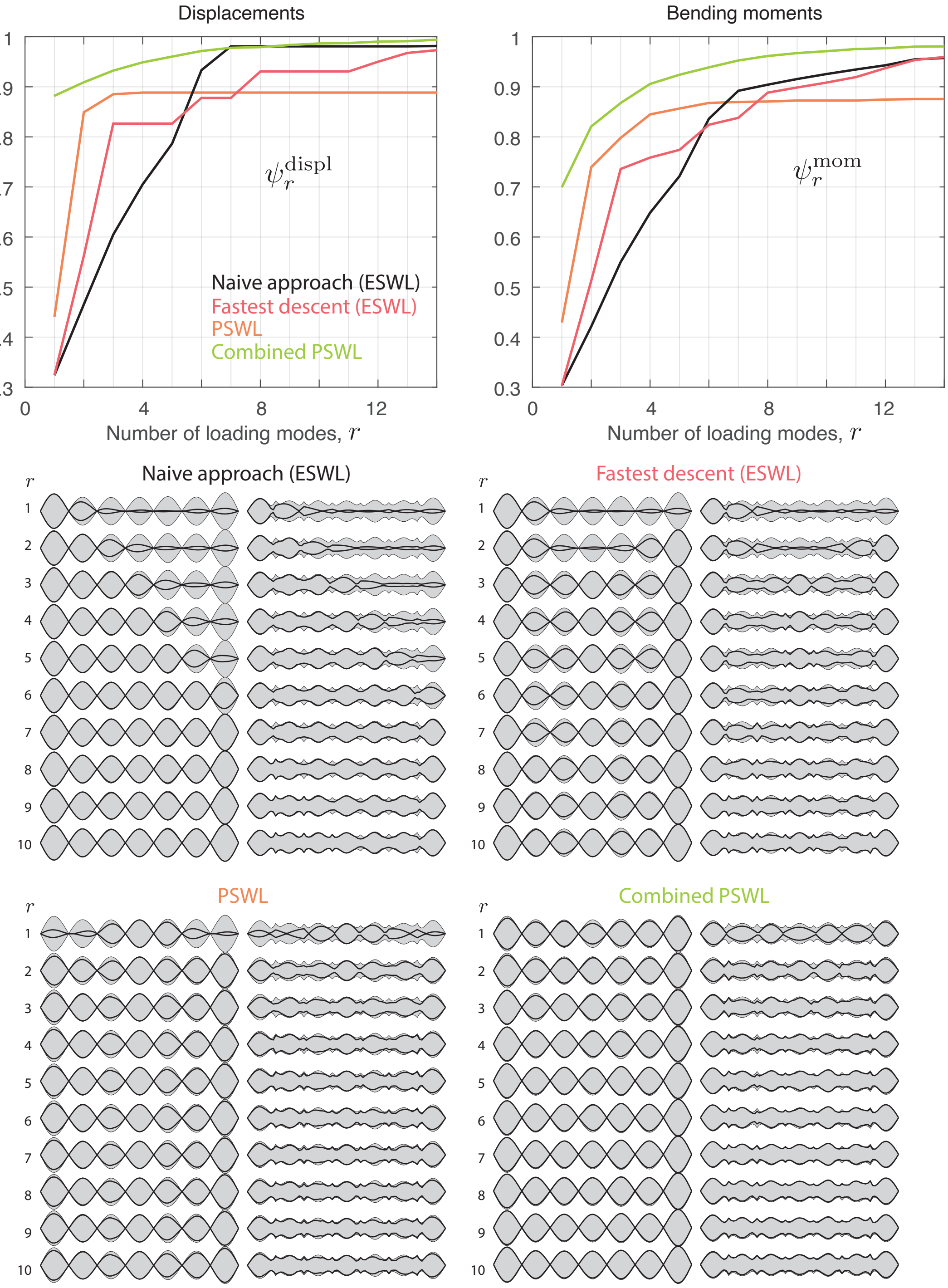

Fig. 6.8: Illustration of the Envelope Reconstruction Problem. Naive approach with ESWLs (§ 5.2.1), fastest descent with ESWLs (§ 5.2.2), based on PSWLs only (§ 5.2.3), based on combinations of PSWLs (§ 5.2.4).

and for $r = 4, 5$ the bending moments on the 3rd and 4th supports. The sequence keep going in an iterative manner, following Algorithm 1. After $r = 10$ iterations, the envelope of the displacement is less well reproduced than with the systematic (naive) approach because some effort has been put on the bending moment diagram. This is illustrated with the reconstructed displacement and bending moment profiles, but also on the top part of the Figure, where the indicator ψ_r^{displ} is seen to decrease very fast for $r \leq 3$, then saturates for $r = 4, 5$, while at the same time ψ_r^{mom} keeps on improving. It could be paradoxical that, for $r \geq 6$, the fastest descent is outperformed by the naive (engineered) approach, especially because the fastest descent choses the best option at each moment to reconstruct the envelope. This is a consequence of the high nonlinearity of the problem. A locally optimal solutions does not always offer the best global performances.

The use of PSWLs (§ 5.2.3) to reconstruct the envelope is illustrated in orange. As shown in Figure 6.7, application of the first PSWL will first reconstruct the midspan displacement in the middle span, and provide a rather fair global reconstruction of bending moment, at least in the three central spans, which is better than the previous two options. After the first three PSWLs ($r = 3$), $\psi_r^{\mathrm{displ}} = 88\%$, which clearly outperforms the first two methods in these first few iterations. For bending moments, ψ_r^{mom} reaches 86% for $r = 5$, which is also much better than for the other two options. Unfortunately, for $r \geq 3$ and $r \geq 7$ respectively, the reconstructions of displacements and bending moments cease to be improved. This is because the PSWLs aim at reconstructing several responses at the same time, and their usage looses track of which response is reconstructed. Therefore, as additional PSWLs are considered to reconstruct the envelope, they might meet the tangency condition for responses that have already been reconstructed during earlier iterations and these PSWLs are just useless. While the sequence of PSWLs offers a very rapid initial convergence, it performs poorly as r approaches the Aerodynamic–Structural Complexity.

Combinations of PSWLs (§ 5.2.4) generalizes the previous approach. It should therefore benefit from the fast initial convergence, but also maintain a fair convergence later in the process since any ESWL can be expressed as a linear combination of PSWLs, at least with a user-defined controlled accuracy. The illustration shows that the envelopes of displacements and bending moments are already fairly well reproduced for $r = 4$ ($\psi_r^{\mathrm{displ}} = 95\%$, $\psi_r^{\mathrm{mom}} = 90\%$). The plots in the upper part of Figure 6.8 also demonstrate the superiority of this method in the reconstruction rate. For this small size problem where only 170 responses are computed and the Aerodynamic-Structural Complexity is equal to 7 (only), the optimal combination coefficients can be determined based on a crude Monte Carlo simulation (see provided Matlab code). This takes a few seconds on a standard personal computer today. For larger models, more advanced techniques based on random walks [215] for instance could drastically improve the computational efficiency and avoid any excessive increase of optimization time.

For completeness, Table 3 reports the numerical values of the reconstruction indices ψ_r^{displ} and ψ_r^{mom} for the four considered reconstructing sequences. Table 4 also reports the combination coefficients obtained in the fourth approach.

7 Acknowledgement

This paper owes its existence to two crucial elements: the gracious invitation extended by the organizing team of ICWE, especially Professors C. Mannini and G. Bartoli, who engaged in insightful discussions, and the invaluable collaboration I shared with Dr. N. Blaise during his doctoral research several years ago.

r	$\psi^{\text{displ}}_{r,(N)}$	$\psi^{\text{displ}}_{r,(F)}$	$\psi^{\text{displ}}_{r,(P)}$	$\psi^{\text{displ}}_{r,(C)}$	$\psi^{\text{mom}}_{r,(N)}$	$\psi^{\text{mom}}_{r,(F)}$	$\psi^{\text{mom}}_{r,(P)}$	$\psi^{\text{mom}}_{r,(C)}$
1	32.4%	32.4%	44.1%	88.1%	30.3%	30.3%	42.9%	69.8%
2	46.5%	56.2%	84.9%	90.8%	42.1%	51.3%	73.9%	82.0%
3	60.5%	82.7%	88.5%	93.1%	55.0%	73.6%	79.8%	86.7%
4	70.5%	82.7%	88.8%	94.8%	64.8%	75.9%	84.5%	90.5%
5	78.6%	82.7%	88.8%	95.9%	72.2%	77.4%	85.7%	92.4%
6	93.3%	87.8%	88.8%	97.0%	83.6%	82.4%	86.8%	93.9%
7	98.1%	87.8%	88.8%	97.7%	89.2%	83.8%	87.0%	95.2%
8	98.1%	93.1%	88.8%	97.8%	90.4%	88.8%	87.1%	96.1%
9	98.1%	93.1%	88.8%	98.2%	91.6%	89.9%	87.3%	96.7%
10	98.1%	93.1%	88.8%	98.5%	92.6%	90.9%	87.3%	97.1%
11	98.1%	93.1%	88.8%	98.6%	93.5%	91.9%	87.3%	97.5%
12	98.1%	95.0%	88.8%	98.9%	94.3%	93.7%	87.5%	97.7%
13	98.1%	96.8%	88.8%	99.0%	95.5%	95.4%	87.5%	98.0%
14	98.2%	97.3%	88.8%	99.3%	95.8%	96.0%	87.5%	98.1%

Tab. 3: Evolution of the reconstruction indicators ψ_r^{displ} and ψ_r^{mom} as a function of r, for the four investigated method (N) Naive approach, (F) Fastest descent, (P) Principal Static Wind Loads, (C) Combinations of PSWLs.

r	PSWL 1	PSWL 2	PSWL 3	PSWL 4	PSWL 5	PSWL 6	PSWL 7
1	0.742	2.109	0.143	-0.019	-0.085	0.309	0.614
2	-1.015	0.043	0.121	-1.176	0.774	-0.632	-0.300
3	-0.773	0.069	-1.746	-0.923	0.814	-0.543	-0.402
4	0.524	-0.069	-2.626	0.132	-0.219	-0.035	-0.487
5	0.460	2.740	-0.617	1.320	0.563	1.141	1.337
6	0.588	-0.182	1.631	0.815	0.003	-0.066	-0.765
7	2.107	-0.405	-0.196	-1.446	0.630	0.986	0.625
8	-0.257	-0.883	-0.304	0.151	-0.351	-0.460	-0.884
9	0.412	0.655	-1.512	-0.465	-1.403	0.068	0.929
10	-0.024	-0.167	-0.906	-1.839	-0.157	0.347	-1.135
11	1.011	1.445	0.317	0.518	-0.205	-1.382	0.014
12	1.377	0.367	-0.542	-0.558	-0.267	-0.275	-0.559
13	0.498	-2.259	-0.550	-0.389	-1.765	-0.175	-1.753
14	0.843	0.421	-0.695	0.380	-0.665	0.477	0.829

Tab. 4: Combination coefficients of the PSWLs offering a faster reconstruction of the envelope. Obtained by Monte Carlo sampling.

8 Conclusion

This article presents a comprehensive overview of methods for determining equivalent static loads (ESWLs) and their application in addressing the envelope reconstruction challenge. Key considerations when selecting among these methods include the structural response type (background, resonant, or mixed) and whether structural properties should be integrated into their determination or solely information pertaining to the wind pressure field. Several methods have been described: those based on the statistical properties of the wind pressure field (GRF and CPT), which are interesting when there is no knowledge about the structural system, the LRC or CST which are interesting when the structural response is quasi-static, the MILs which are interesting when the structural response is purely resonant. We also discussed mixed combinations applicable in the most general case, or even discussed the DRC method, even more general and in principle able to deal with slightly non Gaussian cases.

Two crucial properties of ESWLs are discussed: the non-overshooting condition, which ensures minimal overestimation of the reconstructed envelope and enhances convergence rates, and the tangency condition, which facilitates the normalization of unscaled load distributions to replicate responses accurately.

The optimal number of equivalent loads is another significant consideration. Minimizing this quantity favors global methods like the Universal Wind Load, whereas constructing a comprehensive set of equivalent wind loads provides thorough coverage, as pursued in this study. By establishing an extensive set of responses, designers mitigate the risk of overlooking structural system details and its vulnerability to aerodynamic loading.

The principal static wind loads are derived from the vast array of ESWLs via singular value decomposition. These loadings represent the minimalistic set of static load distributions necessary to reproduce all ESWLs with specified accuracy. We have introduced in this paper the important notion of Aerodynamic–Structural Complexity which corresponds to the truncation order after which the corresponding singular values become unimportant. This notion of Aerodynamic–Structural Complexity is an intrinsic property of both the structure and its aerodynamic loading.Although modern computing power facilitates rapid execution of this task, the method's strength lies in its reliance on comprehensive information, followed by information reduction through principal component analysis.

While ESWLs based solely on aerodynamic properties or in combination with principal static wind loads are viable, the latter prove particularly effective for envelope reconstruction. Their rapid initial reconstruction followed by gradual convergence allows for natural adaptation of combination coefficients to refine inaccurately reconstructed responses. Also, facilitating communication between wind and structural engineers, this approach streamlines the process efficiently. The method described in Section 5.2.4 is clearly the most advanced approach to efficiently tackle the envelope reconstruction problem in complex configurations, ie. complex structural behavior and complex wind loading. Its implementation is systematic are does not necessitate engineering choice. However, in simple cases, it degenerates into well-known methods, and implementing this complete solution is unnecessarily complex for regular designs.

Although the solutions presented in this paper address current challenges, future endeavors may reconsider reconstructing non-symmetric envelopes, nonlinear responses, influence of multiple wind incidences, application to aeroelastic problems [94, 216], interferences [217] and potentially leveraging artificial intelligence algorithms to optimize combination coefficients for reconstruction. In doing so, designs based on ESWL would still be in the race against database-assisted designs which gained interest in the recent years [218, 219, 220]

References

[1] Vincent Denoël et René Maquoi : The concept of numerical admittance. *Archive of Applied Mechanics*, 82:1337–1354, 2012.

[2] N. Blaise et V. Denoël : Principal static wind loads. *Journal of Wind Engineering and Industrial Aerodynamics*, 113:29–39, 2013.

[3] N. Blaise, T. Canor et V. Denoël : Reconstruction of the envelope of non-gaussian structural responses with principal static wind loads. *Journal of Wind Engineering and Industrial Aerodynamics*, 149:59–76, 2016.

[4] Ahsan Kareem et Yukio Tamura : *Advanced structural wind engineering*, volume 482. Springer, 2013.

[5] Emil Simiu et Robert H Scanlan : *Wind effects on structures: fundamentals and applications to design*, volume 688. John Wiley New York, 1996.

[6] John D Holmes, Carol Paton et Robert Kerwin : *Wind loading of structures*. CRC press, 2007.

[7] R.W. Clough et J. Penzien : *Dynamics of Structures*. Civil engineering series. McGraw-Hill, 1993.

[8] K. Aas-Jakobsen et E. Strømmen : Time domain calculations of buffeting response for wind-sensitive structures. *Journal of Wind Engineering and Industrial Aerodynamics*, 74-76:687–695, 1998.

[9] Giovanni Solari : 3-d response of buildings to wind action. *Journal of Wind Engineering and Industrial Aerodynamics*, 23:379–393, 1986.

[10] Emil Simiu : Equivalent static wind loads for tall building design. *Journal of the Structural Division*, 102(4):719–737, 1976.

[11] A. G. Davenport : Gust loading factors. *ASCE Journal of the Structural Engineering Division*, 93(1):11–34, 1967.

[12] V. Denoël : Multiple timescale spectral analysis. *Probabilistic Engineering Mechanics*, 39:69–86, 2015.

[13] V. Denoël : Estimation of modal correlation coefficients from background and resonant responses. *Structural Engineering and Mechanics: an International Journal*, 32(6), 2009.

[14] G. Solari : Wind response spectrum. *Journal of Engineering Mechanics*, 115(9):2057–2073, 1989.

[15] G. Solari : Gust buffeting. ii: Dynamic alongwind response. *Journal of Structural Engineering (United States)*, 119(2):383–398, 1993.

[16] G. Solari : Equivalent wind spectrum technique: Theory and applications. *Journal of Structural Engineering (United States)*, 114(6):1303–1323, 1988.

[17] G. Solari et P. Martín : Gust buffeting and aerodynamic admittance of structures with arbitrary mode shapes. i: Enhanced equivalent spectrum technique. *Journal of Engineering Mechanics*, 147(1), 2021.

[18] JH Lin, YH Zhang et Y Zhao : Pseudo excitation method and some recent developments. *Procedia Engineering*, 14:2453–2458, 2011.

[19] JH Lin, YH Zhang, Q Sh Li et Frederic Ward Williams : Seismic spatial effects for long-span bridges, using the pseudo excitation method. *Engineering Structures*, 26(9):1207–1216, 2004.

[20] R. Dong, Y. Ge et Y. Yang : Multi-target equivalent static wind loading of long-span bridges based on pseudo-excitation method and displacement responses. *Tumu Gongcheng Xuebao/China Civil Engineering Journal*, 47(11):84–91, 2014.

[21] Kurtis R Gurley, Michael A Tognarelli et Ahsan Kareem : Analysis and simulation tools for wind engineering. *Probabilistic Engineering Mechanics*, 12(1):9–31, 1997.

[22] Massimiliano Gioffrè, Vittorio Gusella et Mircea Grigoriu : Non-gaussian wind pressure on prismatic buildings. ii: Numerical simulation. *Journal of Structural Engineering*, 127(9):990–995, 2001.

[23] M. Esposito Marzino et V. Denoël : Non-gaussian buffeting analysis of large structures by means of a proper orthogonal decomposition. *Journal of Wind Engineering and Industrial Aerodynamics*, 242:105576, 2023.

[24] Mircea Grigoriu : Random vibration of mechanical and structural systems. *NASA STI/Recon Technical Report A*, 93:14690, 1993.

[25] Jan Beirlant, Yuri Goegebeur, Johan Segers et Jozef L Teugels : *Statistics of extremes: theory and applications*. John Wiley & Sons, 2006.

[26] Alan Garnett Davenport : Note on the distribution of the largest value of a random function with application to gust loading. *Proceedings of the Institution of Civil Engineers*, 28(2):187–196, 1964.

[27] Xinlai Peng, Luping Yang, Eri Gavanski, Kurtis Gurley et David Prevatt : A comparison of methods to estimate peak wind loads on buildings. *Journal of wind engineering and industrial aerodynamics*, 126:11–23, 2014.

[28] Mircea Grigoriu : Crossings of non-gaussian translation processes. *Journal of Engineering Mechanics*, 110(4):610–620, 1984.

[29] Dae Kun Kwon et Ahsan Kareem : Peak factors for non-gaussian load effects revisited. *Journal of Structural Engineering*, 137(12):1611–1619, 2011.

[30] Min Liu, Xinzhong Chen et Qingshan Yang : Estimation of peak factor of non-gaussian wind pressures by improved moment-based hermite model. *Journal of Engineering Mechanics*, 143(7): 06017006, 2017.

[31] Luping Yang, Kurtis R Gurley et David O Prevatt : Probabilistic modeling of wind pressure on low-rise buildings. *Journal of Wind Engineering and Industrial Aerodynamics*, 114:18–26, 2013.

[32] Emil Simiu et N Alan Heckert : Extreme wind distribution tails: a "peaks over threshold" approach. *Journal of structural engineering*, 122(5):539–547, 1996.

[33] Arvid Næss et Oleg Gaidai : Estimation of extreme values from sampled time series. *Structural safety*, 31(4):325–334, 2009.

[34] Mircea Grigoriu : *Stochastic calculus: applications in science and engineering*. Springer Science & Business Media, 2013.

[35] G. Solari : Design wind loads. *Journal of Wind Engineering and Industrial Aerodynamics*, 11(1-3):345–358, 1983.

[36] A. G. Davenport : The representation of the dynamic effects of turbulent wind by equivalent static wind loads. *In Proceedings of the International Engineering Symposium on Structural Steel*, pages 1–13, Chicago, 1985.

[37] J. D. Holmes : Optimized peak load distributions. *Journal of Wind Engineering and Industrial Aerodynamics*, pages 267–276, 1992.

[38] S. Schmidt et G. Solari : 3-d wind-induced effects on bridges during balanced cantilever erection stages. *Wind and Structures, An International Journal*, 6(1):1–22, 2003.

[39] A Katsumura, Y Tamura et O Nakamura : Universal wind load distribution simultaneously reproducing maximum load effects in all subject members on large-span cantilevered roof. *In Proceedings of the 4th European-African Conference on Wind Engineering*, page 168, 2005.

[40] A Katsumura, Y Tamura et O Nakamura : Universal wind load distribution simultaneously reproducing largest load effects in all subject members on large-span cantilevered roof. *Journal of Wind Engineering and Industrial Aerodynamics*, 95(9-11):1145–1165, 2007.

[41] G. Solari, L. Carassale et F. Tubino : Proper orthogonal decomposition in wind engineering. part 1: A state-of-the-art and some prospects. *Wind and Structures, An International Journal*, 10(2):153–176, 2007.

[42] L. Carassale, G. Solari et F. Tubino : Proper orthogonal decomposition in wind engineering. part 2: Theoretical aspects and some applications. *Wind and Structures, An International Journal*, 10(2):177–208, 2007.

[43] Gal Berkooz, Philip Holmes et John L Lumley : The proper orthogonal decomposition in the analysis of turbulent flows. *Annual review of fluid mechanics*, 25(1):539–575, 1993.

[44] John L Lumley : *Stochastic tools in turbulence*. Courier Corporation, 2007.

[45] Xinzhong Chen et Ahsan Kareem : Proper orthogonal decomposition-based modeling, analysis, and simulation of dynamic wind load effects on structures. *Journal of Engineering Mechanics*, 131(4):325–339, 2005.

[46] Y. Tamura, S. Suganuma, H. Kikuchi et K. Hibi : Proper orthogonal decomposition of random wind pressure field. *Journal of Fluids and Structures*, 13(7-8):1069–1095, 1999.

[47] Peter J Schmid : Dynamic mode decomposition and its variants. *Annual Review of Fluid Mechanics*, 54:225–254, 2022.

[48] Giovanni Solari et Luigi Carassale : Modal transformation tools in structural dynamics and wind engineering. *Wind & Structures*, 3(4):221–241, 2000.

[49] CEN European Committee for Standardization : Eurocode 1: Actions on structures - part 1-4. general actions, wind actions. *(EN 1991-1-4)*, 2005.

[50] G. Solari : Gust buffeting of slender structures and structural elements: Simplified formulas for design calculations and code provisions. *Journal of Structural Engineering (United States)*, 144(2), 2018.

[51] A. Kareem et Y. Zhou : Gust loading factor - past, present and future. *Journal of Wind Engineering and Industrial Aerodynamics*, 91(12-15):1301–1328, 2003.

[52] R. G. J. Flay : *The gust factor approach to evaluate the along-wind response of structures to wind excitation*, pages 157–176. Advanced Structural Wind Engineering. 2013.

[53] A. G. Davenport : Gust response factors for transmission line loading. *Zement-Kalk-Gips*, 2:899–909, 1980.

[54] Y. Uematsu, M. Yamada et A. Karasu : Design wind loads for structural frames of flat long-span roofs: Gust loading factor for the beams supporting roofs. *Journal of Wind Engineering and Industrial Aerodynamics*, 66(1):35–50, 1997.

[55] Y. Uematsu, M. Yamada et A. Karasu : Design wind loads for structural frames of flat long-span roofs: Gust loading factor for a structurally integrated type. *Journal of Wind Engineering and Industrial Aerodynamics*, 66(2):155–168, 1997.

[56] Z. Cao, N. Su, Y. Wu et S. Peng : Gust response envelope approach to the equivalent static wind load for large-span grandstand roofs. *Journal of Wind Engineering and Industrial Aerodynamics*, 180:108–121, 2018.

[57] Ning Su, Shitao Peng et Ningning Hong : Analyzing the background and resonant effects of wind-induced responses on large-span roofs. *Journal of Wind Engineering and Industrial Aerodynamics*, 183:114 – 126, 2018. Cited by: 11.

[58] Wuyi Sun, Xiaomei Wang, Daojun Dong, Meixia Zhang et Qiusheng Li : A comprehensive review on estimation of equivalent static wind loads on long-span roofs. *Advances in Structural Engineering*, 26(14):2572–2599, 2023.

[59] G. Wang, H. Wang, W. Li et F. Zhang : Analysis of wind-induced responses and glf for super-large cooling towers. *Journal of Wind Engineering and Industrial Aerodynamics*, 208, 2021.

[60] A. Fiore et P. Monaco : Pod-based representation of the alongwind equivalent static force for long-span bridges. *Wind and Structures, An International Journal*, 12(3):239–257, 2009.

[61] R. Dong, Y. Ge, Y. Yang et J. Wei : Multi-target equivalent static wind loads of long-span bridges based on proper orthogonal modes. *Tumu Gongcheng Xuebao/China Civil Engineering Journal*, 52(7):110–117, 2019.

[62] Q. Yang, B. Chen et Y. Wu : Wind-induced responses and equivalent static wind loads of long span roofs based on ritz-pod method. *Jianzhu Jiegou Xuebao/Journal of Building Structures*, 32(12):127–136, 2011.

[63] Q. Yang, B. Chen, Y. Wu et Y. Tamura : Wind-induced response and equivalent static wind load of long-span roof structures by combined ritz-proper orthogonal decomposition method. *Journal of Structural Engineering (United States)*, 139(6):997–1008, 2013.

[64] B. Kim, K. T. Tse et Y. Tamura : Pod analysis for aerodynamic characteristics of tall linked buildings. *Journal of Wind Engineering and Industrial Aerodynamics*, 181:126–140, 2018.

[65] Y. Cao, X. Liu, D. Zhou et H. Ren : Investigation of local severe suction on the side walls of a high-rise building by standard, spectral and conditional pod. *Building and Environment*, 217, 2022.

[66] Bubryur Kim et Kam Tim Tse : Pod analysis of aerodynamic correlations and wind-induced responses of two tall linked buildings. *Engineering Structures*, 176:369–384, 2018.

[67] M. Kasperski et H. J. Niemann : Identificatton of critical load distributions for wind loading. *In Proceedings of the 5th International Conference on Structural Safety and Reliability, ICOSSAR89*, San Francisco. CA. USA, 1989.

[68] M. Kasperski et H.-J. Niemann : The lrc (load-response- correlation) method: a general method of estimating unfavorable wind load distributions for linear and nonlinear structural behavior. *Journal of Wind Engineering and Industrial Aerodynamics*, 43:1753–1763, 1992.

[69] H. . Niemann et W. Hubert : Revised wind loading for linear and non-linear design of cooling towers. *In Research and Applications in Structural Engineering, Mechanics and Computation - Proceedings of the 5th International Conference on Structural Engineering, Mechanics and Computation, SEMC 2013*, pages 639–644, 2013.

[70] Hans-Jürgen Niemann : Wind effects on cooling-tower shells. *Journal of the Structural Division*, 106(3):643–661, 1980.

[71] S Papoulis : *Probability, Random Variables and Stochastic Processes by Athanasios.* Boston: McGraw-Hill, 2002.

[72] JD Holmes : Distribution of peak wind loads on a low-rise building. *Journal of Wind Engineering and Industrial Aerodynamics*, 29(1-3):59–67, 1988.

[73] J. D. Holmes : Effective static load distributions in wind engineering. *Journal of Wind Engineering and Industrial Aerodynamics*, 90(2):91–109, 2002.

[74] John D Holmes : Modern techniques for effective wind load distributions on large roofs. *In World Congress on Advances in Civil, Environmental and Materials Research, Seoul, Korea*, 2012.

[75] J. Kim, D. Kim et S. Kim : A study on actual wind load distributions derived by advanced conditional sampling method. *In Proceedings of the Structures Congress and Exposition*, volume 2006, page 15, 2006.

[76] K. Nakao et Y. Hattori : Reconciliation of computational fluid dynamics and observations in complex terrain through conditional resampling. *Journal of Wind Engineering and Industrial Aerodynamics*, 195, 2019.

[77] G. . Shen, N. . Wang, B. . Sun et W. . Lou : Calculation of wind-induced responses and equivalent static wind loads of high-rise buildings based on wind tunnel tests. *Zhejiang Daxue Xuebao (Gongxue Ban)/Journal of Zhejiang University (Engineering Science)*, 46(3):448–453, 2012.

[78] Nicolas Blaise : *Principal static wind loads within a rigorous methodology to the envelope reconstruction problem.* Thèse de doctorat, University of Liège, 2016.

[79] J. Yang, J. Zhang et C. Li : Research on equivalent static load of high-rise/towering structures based on wind-induced responses. *Applied Sciences (Switzerland)*, 12(8), 2022.

[80] Y. Tamura, H. Kikuchi et K. Hibi : Actual extreme pressure distributions and lrc formula. *Journal of Wind Engineering and Industrial Aerodynamics*, 90(12-15):1959–1971, 2002.

[81] R. Dong, Y. Ge, L. Zhao et J. Wei : General expression of lrc method in estimation of bridge's equivalent static wind load. *Journal of Harbin Institute of Technology (New Series)*, 28(3):28–44, 2021.

[82] Z. . Xie, X. . Fang et Z. . Ni : Equivalent static wind loads on tall building-the extended load-response-correlation (elrc) approach. *Zhendong Gongcheng Xuebao/Journal of Vibration Engineering*, 21(4):398–403, 2008.

[83] X. Zhou, M. Gu et G. Li : Grouping response method for equivalent static wind loads based on a modified lrc method. *Earthquake Engineering and Engineering Vibration*, 11(1):107–119, 2012.

[84] X. . Zhou, M. Gu et G. Li : Response grouping method for calculating equivalent static wind loads based on modified lrc. *Zhendong Gongcheng Xuebao/Journal of Vibration Engineering*, 23(2):158–166, 2010.

[85] M. Kasperski : Extreme wind load distributions for linear and nonlinear design. *Engineering Structures*, 14(1):27–34, 1992.

[86] J. D. Holmes : Equivalent static load distributions for resonant dynamic response of bridges. *In Proceedings of the 10th International Conference on Winf Engineering*, pages 907–911, 1999.

[87] S. . Ke, Y. . Ge, L. Zhao, J. . Zhang et Y. Tamura : Proposition and application of consistent coupling method in wind-induced response of long span structures. *Zhongnan Daxue Xuebao (Ziran Kexue Ban)/Journal of Central South University (Science and Technology)*, 43(11):4457–4463, 2012.

[88] Y. Tamura, Y. C. Kim, H. Kikuchi et K. Hibi : Correlation and combination of wind force components and responses. *Journal of Wind Engineering and Industrial Aerodynamics*, 125:81–93, 2014.

[89] X. Chen et A. Kareem : Coupled dynamic analysis and equivalent static wind loads on buildings with three-dimensional modes. *Journal of Structural Engineering*, 131(7):1071–1082, 2005.

[90] Y. Li, Q. Yang et Y. Tian : *Multi-object resonant response equivalent static wind load of large-span roofs*, volume 99-100 de *Applied Mechanics and Materials*. 2011.

[91] J. D. Holmes : Discussion on "how can we simplify and generalize wind loads?" by a.g. davenport. *Journal of Wind Engineering and Industrial Aerodynamics*, 58(1-2):139–141, 1995.

[92] Alan Garnett Davenport : The application of statistical concepts to the wind loading of structures. *Proceedings of the Institution of Civil Engineers*, 19(4):449–472, 1961.

[93] P. Irwin : *Bridge Aerodynamics*, chapitre The role of wind tunnel modeling in the prediction of wind effects on bridges, pages 59–85. Balkema, 1998.

[94] J. P. C. King : Integrating wind tunnel tests of full aeroelastic models into the design of long span bridges. *In Proceedings of the 10th International Conference on Winf Engineering*, pages 927–934, Copenhagen, 1999.

[95] X. Chen et A. Kareem : Equivalent static wind loads for buffeting response of bridges. *Journal of Structural Engineering*, 127(12):1467–1475, 2001.

[96] Y. Zhou, A. Kareem et M. Gu : Equivalent static buffeting loads on structures. *Journal of structural engineering New York, N.Y.*, 126(8):989–992, 2000.

[97] X. Chen et A. Kareem : Equivalent static wind loads on buildings: New model. *Journal of Structural Engineering*, 130(10):1425–1435, 2004.

[98] X. Chen et A. Kareem : Evaluation of equivalent static wind loads on buildings. *In 10th Americas Conference on Wind Engineering, ACWE 2005*, 2005.

[99] Y. Zhou, M. Gu et H. Xiang : Alongwind static equivalent wind loads and responses of tall buildings. part i: Unfavorable distributions of static equivalent wind loads. *Journal of Wind Engineering and Industrial Aerodynamics*, 79(1-2):135–150, 1999.

[100] Y. Zhou, M. Gu et H. Xiang : Alongwind static equivalent wind loads and responses of tall buildings. part ii: Effects of mode shapes. *Journal of Wind Engineering and Industrial Aerodynamics*, 79(1-2):151–158, 1999.

[101] Y. Quan et M. Gu : Across-wind equivalent static wind loads and responses of super-high-rise buildings. *Advances in Structural Engineering*, 15(12):2145–2155, 2012.

[102] G. Huang et X. Chen : Wind load effects and equivalent static wind loads of tall buildings based on synchronous pressure measurements. *Engineering Structures*, 29(10):2641–2653, 2007.

[103] J. D. Holmes : Codification of wind loads on wind-sensitive structures. *International Journal of Space Structures*, 24(2):87–95, 2009.

[104] Y. Tamura, A. Kareem, G. Solari, K. C. S. Kwok, J. D. Holmes et W. H. Melbourne : Aspects of the dynamic wind-induced response of structures and codification. *Wind and Structures, An International Journal*, 8(4):251–268, 2005.

[105] Y. Tamura, H. Kawai, Y. Uematsu, H. Marukawa, K. Fujii et Y. Taniike : Wind load and wind-induced response estimations in the recommendations for loads on buildings, aij 1993. *Engineering Structures*, 18(6):399–411, 1996.

[106] X. Zhou et M. Gu : An approximation method for computing the dynamic responses and equivalent static wind loads of large-span roof structures. *International Journal of Structural Stability and Dynamics*, 10(5):1141–1165, 2010.

[107] J. Fu, Z. Xie, Q. Li, J. Wu et A. Xu : Equivalent static wind loads on long-span roof structures with modal response correlations. *Lixue Xuebao/Chinese Journal of Theoretical and Applied Mechanics*, 39(6):781–787, 2007.

[108] X. Chen et A. Kareem : Evaluation of multimode coupled bridge response and equivalent static wind loading. *In 10th Americas Conference on Wind Engineering, ACWE 2005*, 2005.

[109] N. Blaise, V. Denoël et T. Canor : Equivalent static wind loads for structures with non-proportional damping. *In Research and Applications in Structural Engineering, Mechanics and Computation - Proceedings of the 5th International Conference on Structural Engineering, Mechanics and Computation, SEMC 2013*, pages 663–668, 2013.

[110] N. Blaise, T. Andrianne et V. Denoël : Extensive wind tunnel measurements to explore the conditional expected load method. *In 7th European and African Conference on Wind Engineering, EACWE 2017*, 2017.

[111] Nicolas Blaise et Vincent Denoël : Adjusted equivalent static wind loads for non-gaussian linear static analysis. *In 14th international conference on wind engineering*, 2015.

[112] Luigi Carassale, Giuseppe Piccardo et Giovanni Solari : Double modal transformation and wind engineering applications. *Journal of engineering mechanics*, 127(5):432–439, 2001.

[113] Y. . Li, L. Wang, Y. Tamura et Z. . Shen : Universal equivalent static wind load estimation for spatial structures based on wind-induced envelope responses. *International Journal of Space Structures*, 26(2):105–116, 2011.

[114] B. Chen, X. . Yan et Q. . Yang : Wind-induced response and universal equivalent static wind loads of single layer reticular dome shells. *International Journal of Structural Stability and Dynamics*, 14(4), 2014.

[115] N. Luo, H. Liao et M. Li : An efficient method for universal equivalent static wind loads on long-span roof structures. *Wind and Structures, An International Journal*, 25(5):493–506, 2017.

[116] W. Sun, M. Gu et X. Zhou : Universal equivalent static wind loads of fluctuating wind loads on large-span roofs based on pod compensation. *Advances in Structural Engineering*, 18(9):1443–1460, 2015.

[117] B. Chen et Q. Yang : Universal equivalent static wind loads of china national stadium. *In 7th Asia-Pacific Conference on Wind Engineering, APCWE-VII*, 2009.

[118] S. Li, X. Zhang, N. Chen, Y. Dai et B. Li : Refined three components method for determining universal equivalent static wind loads of large span roof. *Yingyong Lixue Xuebao/Chinese Journal of Applied Mechanics*, 34(6):1072–1078, 2017.

[119] V. Denoël : On the background and biresonant components of the random response of single degree-of-freedom systems under non-gaussian random loading. *Engineering structures*, 33(8):2271–2283, 2011.

[120] W. Lou, L. Zhang, M. F. Huang et Q. S. Li : Multiobjective equivalent static wind loads on complex tall buildings using non-gaussian peak factors. *Journal of Structural Engineering (United States)*, 141(11), 2015.

[121] W. Kassir, C. Soize, J. . Heck et F. De Oliveira : Non-gaussian approach for equivalent static wind loads from wind tunnel measurements. *Wind and Structures, An International Journal*, 25(6):589–609, 2017.

[122] W. Kassir, C. Soize, J. . Heck et F. D. Oliveira : A non-gaussian probabilistic approach for estimating the equivalent static wind loads on structures from unsteady pressure field. *In 7th European and African Conference on Wind Engineering, EACWE 2017*, 2017.

[123] L. Patruno, M. Ricci et S. de Miranda : Buffeting analysis: a numerical study on the extraction of equivalent static wind loads. *Meccanica*, 53(4-5):671–680, 2018.

[124] L. Patruno, M. Ricci, S. de Miranda et F. Ubertini : An efficient approach to the determination of equivalent static wind loads. *Journal of Fluids and Structures*, 68:1–14, 2017.

[125] M. M. Salehinejad et R. G. J. Flay : A review of approaches to generate equivalent static and synthetic wind loads on tall buildings for the preliminary stage of design. *Journal of Wind Engineering and Industrial Aerodynamics*, 219, 2021.

[126] C. . Cheng, T. . Lai, J. Wang et M. . Tsai : An acrosswind equivalent static wind load model for rectangular shaped tall buildings. *Journal of the Chinese Institute of Civil and Hydraulic Engineering*, 31(8):759–766, 2019.

[127] C. M. Cheng, J. Wang et T. C. Lai : An acrosswind equivalent static wind load model for rectangular shaped tall buildings. *In 9th Asia Pacific Conference on Wind Engineering, APCWE 2017*, 2017.

[128] S. Liang, L. Zou, D. Wang et G. Huang : Analysis of three dimensional equivalent static wind loads of symmetric high-rise buildings based on wind tunnel tests. *Wind and Structures, An International Journal*, 19(5):565–583, 2014.

[129] G. Piccardo et G. Solari : A refined model for calculating 3-d equivalent static wind forces on structures. *Journal of Wind Engineering and Industrial Aerodynamics*, 65(1-3):21–30, 1996.

[130] S. Ke, H. Wang et Y. Ge : Wind load effects and equivalent static wind loads of three-tower connected tall buildings based on wind tunnel tests. *Structural Engineering and Mechanics*, 58(6): 967–988, 2016.

[131] X. Pan, J. Song, W. Qu, L. Zou et S. Liang : An improved derivation and comprehensive understanding of the equivalent static wind loads of high-rise buildings with structural eccentricities. *Structural Design of Tall and Special Buildings*, 31(17), 2022.

[132] G. . Shen, B. . Sun et W. . Lou : Simple method to calculate the equivalent static wind load on low-rise buildings. *Gongcheng Lixue/Engineering Mechanics*, 23(SUPPL.):163–168, 2006.

[133] X. Chen, N. Zhou et D. A. Smith : Equivalent static wind loads on low-rise buildings based on full scale measurements. *In Proceedings of the Structures Congress and Exposition*, volume 2006, page 16, 2006.

[134] X. Chen et N. Zhou : Equivalent static wind loads on low-rise buildings based on full-scale pressure measurements. *Engineering Structures*, 29(10):2563–2575, 2007.

[135] B. Chen, Q. Yang et Y. Wu : Wind-induced response and equivalent static wind loads of long span roofs. *Advances in Structural Engineering*, 15(7):1099–1114, 2012.

[136] J. Fu, Z. Xie et Q. S. Li : Closure to "equivalent static wind loads on long-span roof structures" by j. fu, z. xie, and q. s. li. *Journal of Structural Engineering*, 136(4):470–471, 2010.

[137] B. Chen, Y. Wu et S. . Shen : Background of equivalent static wind loads on large span roofs. *Gongcheng Lixue/Engineering Mechanics*, 23(11):21–27, 2006.

[138] M. Gu et Y. Huang : Equivalent static wind loads for stability design of large span roof structures. *Wind and Structures, An International Journal*, 20(1):95–115, 2015.

[139] J. Holmes et G. Wood : The determination of structural wind loads for the roofs of several venues for the 2000 olympics. *In Structures - A Structural Engineering Odyssey, Structures 2001 - Proceedings of the 2001 Structures Congress and Exposition*, volume 109, 2004.

[140] F. . Li, Z. . Ni et S. . Shen : Equivalent static wind loads on long span roofs. *Gongcheng Lixue/Engineering Mechanics*, 24(7):104–109+127, 2007.

[141] M. Duan, Z. . Ni et Z. . Xie : Envelope equivalent static wind load distribution on large roofs. *Zhendong yu Chongji/Journal of Vibration and Shock*, 27(9):6–10, 2008.

[142] A. Katsumura, Y. Tamura et O. Nakamura : Maximum wind load effects on a large-span cantilevered roof. *Structural Engineering International: Journal of the International Association for Bridge and Structural Engineering (IABSE)*, 15(4):248–251, 2005.

[143] C. W. Letchford et G. P. Killen : Equivalent static wind loads for cantilevered grandstand roofs. *Engineering Structures*, 24(2):207–217, 2002.

[144] Z. Wang, X. Wang, H. Zhao, B. Chen et Q. Yang : Equivalent static wind loads on canopies of regular railway stations. *Engineering Structures*, 276, 2023.

[145] Y. L. Lo et C. H. Wu : *Estimations for equivalent static wind loads of dome roof structures*, volume 101 de *Lecture Notes in Civil Engineering*. 2021.

[146] S. . Ke, S. . Chen et Y. . Ge : Wind-induced response and equivalent static wind load for suspended dome roof structure of jinan olympic sports hall. *Zhendong Gongcheng Xuebao/Journal of Vibration Engineering*, 26(2):214–219, 2013.

[147] Z. H. Zhang et Y. Tamura : Wind tunnel tests and wind-induced vibration analysis of spherical domes. *Advanced Steel Construction*, 2(1):71–86, 2006.

[148] N. Luo, H. . Liao et M. . Li : Universal equivalent static wind loads for long-span roofs in time domain. *Gongcheng Lixue/Engineering Mechanics*, 30(4):316–321, 2013.

[149] W. . Sun, X. . Zhou et M. Gu : Equivalent static wind loads of fluctuating wind on large-span roofs based on compensated method. *Zhendong Gongcheng Xuebao/Journal of Vibration Engineering*, 24(6):658–663, 2011.

[150] W. . Sun, X. . Zhou et M. Gu : Equivalent static wind loads of fluctuating wind on large-span roofs based on eigen-mode compensation. *Gongcheng Lixue/Engineering Mechanics*, 28(4):96–101, 2011.

[151] W. Sun et Q. Zhang : Universal equivalent static wind loads of fluctuating wind loads on large-span roofs based on compensation of structural frequencies and modes. *Structures*, 26:92–104, 2020.

[152] L. Patruno, M. Ricci, S. de Miranda et F. Ubertini : Equivalent static wind loads: Recent developments and analysis of a suspended roof. *Engineering Structures*, 148:1–10, 2017.

[153] N. Luo, H. Jia et H. Liao : Coupled wind-induced responses and equivalent static wind loads on long-span roof structures with the consistent load–response–correlation method. *Advances in Structural Engineering*, 21(1):71–81, 2018.

[154] B. Chen, Y. Wu et S. . Shen : Study of the resonant component of equivalent static wind loads on large span roofs. *Gongcheng Lixue/Engineering Mechanics*, 24(1):51–55+66, 2007.

[155] X. Li et Z. Xie : Efficient algorithm and application for the wind-induced response and equivalent static wind load of large-span roof structures. *Tumu Gongcheng Xuebao/China Civil Engineering Journal*, 43(7):29–36, 2010.

[156] Murray J Morrison et Gregory A Kopp : Analysis of wind-induced clip loads on standing seam metal roofs. *Journal of structural engineering*, 136(3):334–337, 2010.

[157] X. Jing et Y. Li : Effective static wind load for clips of standing seam roof system. *Tongji Daxue Xuebao/Journal of Tongji University*, 41(11):1630–1635+1760, 2013.

[158] B. Chen, H. Zhao, X. Wang et Z. Wang : Wind-induced response and equivalent static wind loads on waiting hall building of regular railway stations. *International Journal of Structural Stability and Dynamics*, 22(14), 2022.

[159] P. Martín et A. El Damatty : Comparison of the canadian standard and other standards for wind loading on self-supporting telecommunication towers. *Canadian Journal of Civil Engineering*, 48(8):993–1003, 2021.

[160] A. S. Ross, A. A. El Damatty et A. M. El Ansary : *Reduced equivalent static wind loads for tall buildings with tuned liquid dampers*, volume 226-228 de *Applied Mechanics and Materials*. 2012.

[161] H. Matsumiya, S. Taruishi, M. Shimizu, G. Sakaguchi et J. H. G. Macdonald : Equivalent static wind loads on snow-accreted overhead wires. *Structural Engineering International*, 32(1):78–91, 2022.

[162] B. Chen, Y. Wu et S. Shen : Equivalent static wind loads on saddle-shaped cable structures. *Tumu Gongcheng Xuebao/China Civil Engineering Journal*, 39(6):1–5+18, 2006.

[163] R. Dong, Y. . Ge, Y. . Yang et J. . Wei : Buffeting equivalent static wind loading calculation method of asymmetric single tower cable-stayed bridges based on multi modes. *Zhongguo Gonglu Xuebao/China Journal of Highway and Transport*, 29(11):108–115, 2016.

[164] J. D. Holmes : Along-wind response of lattice towers - iii. effective load distributions. *Engineering Structures*, 18(7):489–494, 1996.

[165] M. Fujimoto, I. Matsushita, T. Ohkuma, T. Amano et H. Akagi : On wind-proof performance of latticed steel towers. *Zement-Kalk-Gips*, 2:1203–1215, 1980.

[166] B. Chen, K. Wang, J. Chao et Q. Yang : Equivalent static wind loads on single-layer cylindrical steel shells. *Journal of Structural Engineering (United States)*, 144(7), 2018.

[167] J. . Zhang, Y. . Ge, L. Zhao et B. Zhu : Wind induced dynamic responses on hyperbolic cooling tower shells and the equivalent static wind load. *Journal of Wind Engineering and Industrial Aerodynamics*, 169:280–289, 2017.

[168] D. Wu, Y. Wu et J. . Zhang : Wind-induced response and equivalent static wind loads of double-layer reticulated shell structures. *Harbin Gongye Daxue Xuebao/Journal of Harbin Institute of Technology*, 42(10):1543–1547, 2010.

[169] S. S. Cao, S. T. Ke, W. M. Zhang, L. Zhao, Y. J. Ge et X. X. Cheng : Load–response correlation–based equivalent static wind loads for large cooling towers. *Advances in Structural Engineering*, 22(11):2464–2475, 2019.

[170] S. T. Ke, Y. J. Ge, L. Zhao et Y. Tamura : A new methodology for analysis of equivalent static wind loads on super-large cooling towers. *Journal of Wind Engineering and Industrial Aerodynamics*, 111:30–39, 2012.

[171] X. X. Cheng, S. T. Ke, P. F. Li, Y. J. Ge et L. Zhao : External extreme wind pressure distribution for the structural design of cooling towers. *Engineering Structures*, 181:336–353, 2019.

[172] R. Feng, J. Ding, Q. Li et J. Ye : Wind-induced response and equivalent static wind load of single-layer geiger lattice shell with curved plate. *Dongnan Daxue Xuebao (Ziran Kexue Ban)/Journal of Southeast University (Natural Science Edition)*, 42(2):328–333, 2012.

[173] Y. . Li et Y. Tamura : Equivalent static wind load estimation in wind-resistant design of single-layer reticulated shells. *Wind and Structures, An International Journal*, 8(6):443–454, 2005.

[174] Y. . Huang, L. Zhong et J. . Fu : Wind-induced vibration and equivalent wind load of double-layer cylindrical latticed shells. *Journal of Vibroengineering*, 16(2):1063–1078, 2014.

[175] N. Ma, X. Wang, R. Hong, D. Zhou, F. Li et J. Ma : Equivalent static wind loads on large-span arched structures. *Shanghai Jiaotong Daxue Xuebao/Journal of Shanghai Jiaotong University*, 50(3):317–323 and 330, 2016.

[176] T. . Ma, L. Zhao, T. . Ji et T. Tang : Case study of wind-induced performance and equivalent static wind loads of large-span openable truss structures. *Thin-Walled Structures*, 175, 2022.

[177] R. Feng, J. Ding, Q. Li et J. Ye : Wind load and equivalent static wind load of single-layer spatial reticulated structure. *Jianzhu Jiegou Xuebao/Journal of Building Structures*, 33(1):58–64, 2012.

[178] N. Ma, X. Wang, D. Zhou, F. Zhu, Z. Wang et R. Hong : Simulation and analysis of wind pressure and equivalent static wind loads of multi-body structure with complex shape. *Shanghai Jiaotong Daxue Xuebao/Journal of Shanghai Jiaotong University*, 50(3):351–356 and 363, 2016.

[179] Z. . Zhong et W. . Lou : Equivalent static wind load on extra-high buildings along wind based on wind-gravity coupling effect. *Gongcheng Lixue/Engineering Mechanics*, 33(5):74–81, 2016.

[180] S. T. Ke, T. G. Wang, Y. J. Ge et Y. Tamura : Wind-induced responses and equivalent static wind loads of tower-blade coupled large wind turbine system. *Structural Engineering and Mechanics*, 52(3):485–505, 2014.

[181] S. . Ke, T. . Wang, S. . Chen et Y. . Ge : Wind-induced responses and equivalent static wind load of large wind turbine system. *Zhejiang Daxue Xuebao (Gongxue Ban)/Journal of Zhejiang University (Engineering Science)*, 48(4):686–692, 2014.

[182] K. Chen, L. Fu, J. Qian et X. Jin : Analysis method of equivalent static wind load on large-span spatial structures based on response time history. *Jianzhu Jiegou Xuebao/Journal of Building Structures*, 33(1):35–42, 2012.

[183] Q. Wang, Z. Li, A. Garg, B. Hazra et Z. Xie : Effects of tuned mass damper on correlation of wind-induced responses and combination coefficients of equivalent static wind loads of high-rise buildings. *Structural Design of Tall and Special Buildings*, 28(6), 2019.

[184] Z. Li, G. Huang, X. Chen, Y. Zhou et Q. Yang : Wind-resistant design and equivalent static wind load of base-isolated tall building: A case study. *Engineering Structures*, 212, 2020.

[185] Y. . Li, Q. . Yang, Y. . Tian et Y. . Zhu : Multiple targets equivalent static wind load for long-span roofs. *Gongcheng Lixue/Engineering Mechanics*, 33(6):85–92, 2016.

[186] Y. Li, Q. Yang, Y. Tian et Y. Zhu : Refinement analysis of multi-target equivalent static wind loads for large-span roofs. *Zhongnan Daxue Xuebao (Ziran Kexue Ban)/Journal of Central South University (Science and Technology)*, 47(7):2485–2494, 2016.

[187] B. Chen, M. Li et Q. . Yang : Equivalent static wind loads of multi-targets for long span plane roofs. *Zhendong yu Chongji/Journal of Vibration and Shock*, 32(24):22–27, 2013.

[188] Nicolas Blaise, Lotfi Hamra et Vincent Denoël : Principal static wind loads on a large roof structure. *In XII Convegno Nazionale di Ingegneria del Vento*, 2012.

[189] Ahsan Kareem : Wind-excited response of buildings in higher modes. *Journal of the Structural Division*, 107(4):701–706, 1981.

[190] G. Solari : The role of analytical methods for evaluating the wind-induced response of structures. *Journal of Wind Engineering and Industrial Aerodynamics*, 90(12-15):1453–1477, 2002.

[191] Gilbert W Stewart : On the early history of the singular value decomposition. *SIAM review*, 35(4):551–566, 1993.

[192] Ian T Jolliffe et Jorge Cadima : Principal component analysis: a review and recent developments. *Philosophical transactions of the royal society A: Mathematical, Physical and Engineering Sciences*, 374(2065):20150202, 2016.

[193] S Kho, Christopher Baker et R Hoxey : Pod/arma reconstruction of the surface pressure field around a low rise structure. *Journal of Wind Engineering and Industrial Aerodynamics*, 90(12-15):1831–1842, 2002.

[194] Dan Ruan, Hua He, David A Castañón et Kishor C Mehta : Normalized proper orthogonal decomposition (npod) for building pressure data compression. *Journal of wind engineering and industrial aerodynamics*, 94(6):447–461, 2006.

[195] Sam Roweis : Em algorithms for pca and spca. *Advances in neural information processing systems*, 10, 1997.

[196] G. Frontini, T. Argentini, L. Rosa et D. Rocchi : Advances in the application of the principal static wind loads: A large-span roof case. *Engineering Structures*, 262, 2022.

[197] Luca Patruno, Mattia Ricci, Stefano de Miranda et Francesco Ubertini : An efficient approach to the evaluation of wind effects on structures based on recorded pressure fields. *Engineering Structures*, 124:207–220, 2016.

[198] N. Blaise, T. Andrianne et V. Denoël : Assessment of extreme value overestimations with equivalent static wind loads. *Journal of Wind Engineering and Industrial Aerodynamics*, 168:123–133, 2017.

[199] X. Zhou, M. Gu et G. Li : Constrained least-squares method for computing equivalent static wind loads of large-span roofs. *Advances in Structural Engineering*, 17(10):1497–1515, 2014.

[200] X. Zhou, M. Gu et G. Li : Weighted constrained least squares method for calculating equivalent static wind loads of large-span roof. *Tongji Daxue Xuebao/Journal of Tongji University*, 38(10):1403–1408, 2010.

[201] B. Chen, M. Li et Q. . Yang : Equivalent static wind loads for multiple targets based on wind-induced response. *Gongcheng Lixue/Engineering Mechanics*, 29(11):152–157+164, 2012.

[202] R. Dong, Y. . Ge et Y. . Yang : Calculation for multi-target equivalent static wind loads of lang-span bridge based on displacement response. *Zhongguo Gonglu Xuebao/China Journal of Highway and Transport*, 26(5):69–75, 2013.

[203] Y. . Li, L. . Feng, H. . Li et Y. . Tian : A practical method for analyzing multiple target equivalent static wind load considering the characteristics of wind-induced response. *Zhendong Gongcheng Xuebao/Journal of Vibration Engineering*, 35(1):140–147, 2022.

[204] M. H. Huang et Y. L. Lo : A refined method of multi-target equivalent static wind loads: A bridge case. *Journal of Wind Engineering and Industrial Aerodynamics*, 212, 2021.

[205] X. Zhou, M. Gu et G. Li : Eswl for large-span roof based on grouping response method. *In Proceedings of the 8th Asia-Pacific Conference on Wind Engineering, APCWE 2013*, pages 1–11, 2013.

[206] Dimitri P Bertsekas : *Constrained optimization and Lagrange multiplier methods.* Academic press, 2014.

[207] Abdollah Homaifar, Charlene X Qi et Steven H Lai : Constrained optimization via genetic algorithms. *Simulation*, 62(4):242–253, 1994.

[208] Efrén Mezura-Montes, Jesús Velázquez-Reyes et CA Coello Coello : Modified differential evolution for constrained optimization. *In 2006 IEEE International Conference on Evolutionary Computation*, pages 25–32. IEEE, 2006.

[209] Edwin KP Chong et Stanislaw H Żak : *An introduction to optimization*, volume 75. John Wiley & Sons, 2013.

[210] Q. Wang, S. Yu, C. Ku et A. Garg : Combination coefficient of eswls of a high-rise building with an elliptical cross-section. *Wind and Structures, An International Journal*, 31(6):523–532, 2020.

[211] Hervé Cardot et David Degras : Online principal component analysis in high dimension: Which algorithm to choose? *International Statistical Review*, 86(1):29–50, 2018.

[212] V. Denoël : Polynomial approximation of aerodynamic coefficients based on the statistical description of the wind incidence. *Probabilistic engineering mechanics*, 24(2):179–189, 2009.

[213] Bernardo Morais da Costa, Jungao Wang, Jasna Bogunović Jakobsen, Ole Andre Øiseth et Jónas Þór Snæbjörnsson : Bridge buffeting by skew winds: A revised theory. *Journal of Wind Engineering and Industrial Aerodynamics*, 220:104806, 2022.

[214] Masanobu Shinozuka et George Deodatis : Simulation of Stochastic Processes by Spectral Representation. *Applied Mechanics Reviews*, 44(4):191–204, 04 1991.

[215] Dimitris Bertsimas et Santosh Vempala : Solving convex programs by random walks. *Journal of the ACM (JACM)*, 51(4):540–556, 2004.

[216] Weiwei Song, Shuguo Liang, Jie Song, Lianghao Zou et Gang Hu : Investigation on wind-induced aero-elastic effects of tall buildings by wind tunnel test using a bi-axial forced vibration device. *Engineering Structures*, 195:414 – 424, 2019. Cited by: 21.

[217] Ying Sun, Zhiyuan Li, Xiaoying Sun, Ning Su et Shitao Peng : Interference effects between two tall chimneys on wind loads and dynamic responses. *Journal of Wind Engineering and Industrial Aerodynamics*, 206, 2020. Cited by: 15.

[218] Sejun Park, Emil Simiu et DongHun Yeo : Equivalent static wind loads vs. database-assisted design of tall buildings: An assessment. *Engineering Structures*, 186:553 – 563, 2019. Cited by: 6.

[219] X. Wang, Z. Huang, B. Chen et Q. Yang : Equivalent static wind loads on plate-like flat roofs: Data-based closed form. *Journal of Structural Engineering (United States)*, 146(6), 2020.

[220] DongHun Yeo, Florian A. Potra et Emil Simiu : Tall building database-assisted design: A review of nist research. *International Journal of High-Rise Buildings*, 8(4):265 – 273, 2019. Cited by: 0.